Journal of Medicinal Chemistry

pubs.acs.org/jmc Article

Fragment-Based Discovery of Novel Non-Hydroxamate LpxC Inhibitors with Antibacterial Activity

Yousuke Yamada,* Hajime Takashima, David Lee Walmsley, Fumihito Ushiyama, Yohei Matsuda, Harumi Kanazawa, Toru Yamaguchi-Sasaki, Nozomi Tanaka-Yamamoto, Junya Yamagishi, Risa Kurimoto-Tsuruta, Yuya Ogata, Norikazu Ohtake, Hayley Angove, Lisa Baker, Richard Harris, Alba Macias, Alan Robertson, Allan Surgenor, Hayato Watanabe, Koichiro Nakano, Masashi Mima, Kunihiko Iwamoto, Atsushi Okada, Iichiro Takata, Kosuke Hitaka, Akihiro Tanaka, Kiyoko Fujita, Hiroyuki Sugiyama, and Roderick E. Hubbard*

Cite This: https://dx.doi.org/10.1021/acs.jmedchem.0c01215 Read Online

ACCESS | Metrics & More | Article Recommendations | Supporting Information

ABSTRACT: UDP-3-*O*-acyl-*N*-acetylglucosamine deacetylase (LpxC) is a zinc metalloenzyme that catalyzes the first committed step in the biosynthesis of Lipid A, an essential component of the cell envelope of Gram-negative bacteria. The most advanced, disclosed LpxC inhibitors showing antibacterial activity coordinate zinc through a hydroxamate moiety with concerns about binding to other metalloenzymes. Here, we describe the discovery, optimization, and efficacy of two series of compounds derived from fragments with differing modes of zinc chelation. A series was evolved from a fragment where a glycine moiety complexes zinc, which achieved low nanomolar potency in an enzyme functional assay but poor antibacterial activity on cell cultures. A second series was based on a fragment that chelated zinc through an imidazole moiety. Structure-guided design led to a 2-(1*S*-hydroxyethyl)-imidazole derivative exhibiting low nanomolar inhibition of LpxC and a minimum inhibitory concentration (MIC) of 4 μg/mL against *Pseudomonas aeruginosa*, which is little affected by the presence of albumin.

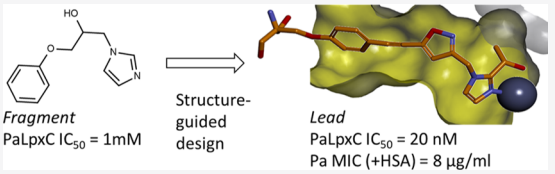

INTRODUCTION

There has been growing concern over the emergence of bacterial resistance to existing therapeutics[1] and the challenges of discovering new antibiotics.[2] An attractive target for the development of novel therapeutic agents is the bacterial enzyme UDP-3-*O*-acyl-*N*-acetylglucosamine deacetylase (LpxC).[3−5] The enzyme is essential to most Gram-negative pathogens,[6,7] catalyzing the removal of an *N*-acetyl group from UDP-3-*O*-acyl-*N*-acetylglucosamine, which forms the core of Lipid A, the first committed step in biosynthesis of the lipopolysaccharide (LPS), which is an essential component of the bacterial cell wall (Figure 1). There are no mammalian homologues, and several series of inhibitors (summarized in ref[3−5]) have been developed (representatives in Figure 2). The most advanced disclosed compounds contain a hydroxamate functionality that complexes the zinc ion at the core of the active site of the metalloenzyme. One of these compounds (ACHN-975[8,9]) entered clinical trials but was discontinued due to side effects not thought to be target-related.[9] Although other properties of ACHN-975 may be important, the hydroxamate moiety has been linked to mutagenicity in HDAC inhibitors[10] and also to be responsible for off-target effects due to the lack of specificity in many matrix metalloprotease (MMP) inhibitors.[11] There is therefore interest in identifying LpxC inhibitors containing non-hydroxamate metal binding groups. Hydroxypyrone-containing compounds such as **2** have been discussed[3] and are proposed to form a bidentate complex with the zinc ion (patent WO 2015/085238 from Forge Therapeutics), and further examples of this motif have been disclosed in pyrone compounds such as **3** (Example 49 in patent WO 2017/083434 from Forge Therapeutics). However, no details of the pyrone-containing compounds have yet been published. Compound **2** is referred to as LpxCi-1 in ref;[3] this should not be confused with a hydroxamate-containing compound named LpxCi-1 in the Achaogen patent WO 2011/005355.

The published crystal structure of **1** (PF-5081090) in the active site of LpxC from *Pseudomonas aeruginosa* (PaLpxC)[12] illustrates key features of inhibitor binding as shown in Figure 3. The protein coordinates the catalytic zinc ion through side chains of D241, H78, and H237 with a trigonal pyramidal geometry. In **1**, the hydroxamate makes a bidentate interaction to complete a trigonal bipyramidal geometry at

Received: July 29, 2020

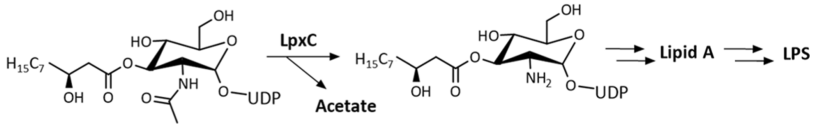

Figure 1. LpxC catalyzes the first committed step of LPS biosynthesis (shown is the substrate for *Pseudomonas aeruginosa*).

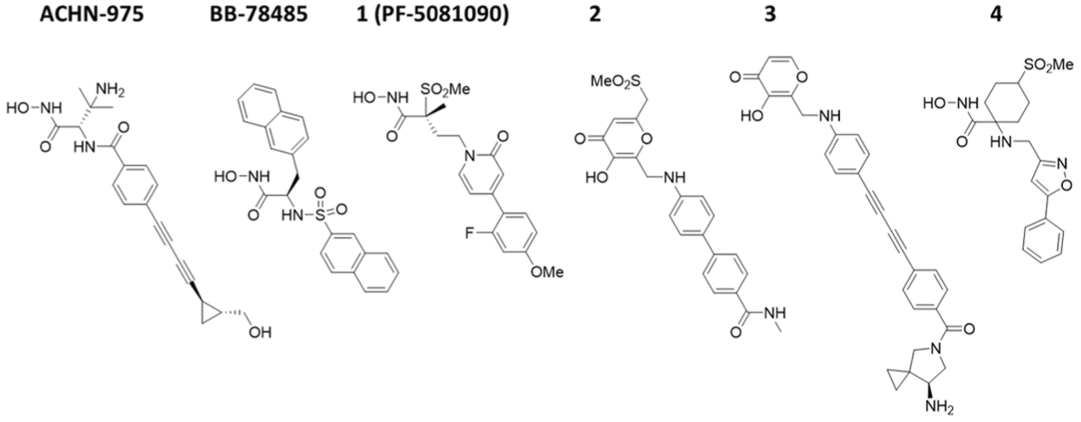

Figure 2. Representative LpxC inhibitors.

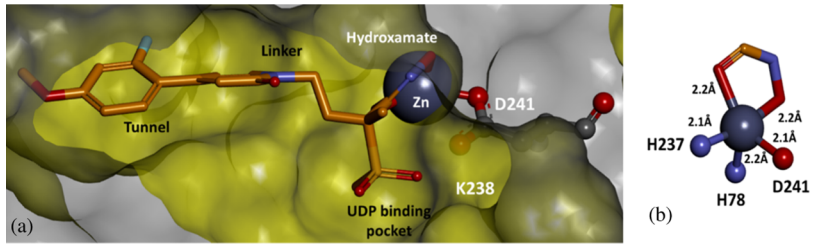

Figure 3. Detail of the crystal structure (PDB code: 5UPG) of **1** (PF-5081090) binding to the active site of PaLpxC. Unless otherwise stated, in all structural figures, compounds are shown by sticks with orange carbons, the zinc ion as a van der Waals sphere, and protein amino acids (side chains only) in ball and stick. Except for (b) and 4(a), all other figures of compounds binding to LpxC are presented with the same view and convention. (a) Inhibitor binding site, with the inside of the solvent surface in gray and the outside in yellow. (b) Detail of inhibitor and protein binding to a zinc ion, showing just the hydroxamate moiety of the ligand, the NE2 atoms of the imidazole of histidines, and one oxygen of the side chain of aspartic acid. Note that **1** also binds in a second site, described as the F181 site later in this manuscript.

the zinc ion, and the pendant sulfone occupies the pocket that binds a phosphate of UDP (see the structure with the PDB code: 4MDT[13]) adjacent to K238. The pyridone ring makes only hydrophobic interactions with the protein binding site, acting as a linker that connects the core zinc-chelating unit to groups that mimic the acyl chain in the natural substrate that binds in a hydrophobic tunnel that leads to the solvent. These features of the binding site are exploited by most published inhibitors: (a) a zinc-chelating motif, (b) a polar group occupying the UDP binding pocket, (c) a linker that is mainly hydrophobic but sometimes makes at least one hydrogen bond interaction, (d) an extended hydrophobic moiety that binds in the tunnel, and (e) often addition of groups out into the solvent at the end of the tunnel to modulate compound properties. Crystal structures of different compounds bound to LpxC from various organisms show variation in the extent and nature of the tunnel, which leads to varying specificity for some compounds for different bacterial species.[3,14]

Here, we report the fragment-based discovery, optimization, and characterization of a potent, non-hydroxamate-containing inhibitor of PaLpxC, which shows efficacy in various measures of antibacterial activity.

RESULTS AND DISCUSSION

Establishing a Structure-Based Discovery Platform. Two constructs of the enzyme were used in the work reported here. A construct for residues 1 to 303 with a C-terminal his-tag (hereafter PaLpxC (1−303-His)) was used for the functional assay. A construct for residues 1 to 299 (based on the published structure, PDB code: 5UPG) was generated with the surface mutation C40S to reduce protein aggregation (hereafter PaLpxC) and used for all structural and biophysical measurements, including the binding assay. Initial attempts to express and purify N-terminal poly-histidine-tagged PaLpxC produced insoluble aggregates. Removing the tag with proteolytic cleavage did not improve the solubility. Expression of untagged PaLpxC with a reduced induction time resulted in a protein that was more soluble but did not generate crystals. Analysis by $^{1}H-^{15}N$ HSQC NMR of a ^{15}N-labeled sample of PaLpxC (Figure S1a) showed fewer amide peaks than expected, suggesting that the protein is partially unfolded; adding zinc improved the $^{1}H-^{15}N$ HSQC NMR (Figure S1b), but the protein still did not form crystals. Thermal shift analysis (TSA) suggested there was still heterogeneity; maintaining zinc in the expression medium resulted in a protein with improved

https://dx.doi.org/10.1021/acs.jmedchem.0c01215
J. Med. Chem. XXXX, XXX, XXX−XXX

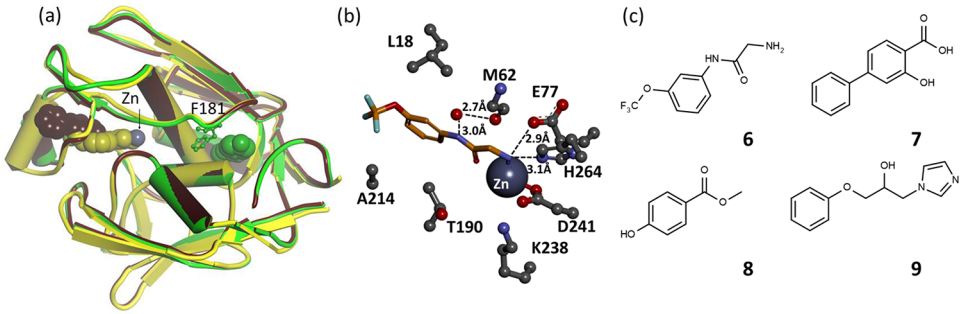

Figure 4. Fragments are found that bind to different sites on LpxC. (a). Schematic of the protein structure, with F181 in ball and stick, with ligand in CPK for the crystal structures of a zinc-coordinating glycine fragment (**6**, yellow), a tunnel binder (**7**, brown), and binding to the F181 site (**8**, green). A second copy (not shown) of **8** binds in the tunnel. (b) Detail of the binding of glycine fragment (**6**) with just the main chain of M62 shown (see Figure 3 for the legend). (c). Representative fragment hits.

Table 1. Glycine Series: SAR for Interacting with Zinc and the Substrate Binding Site

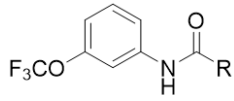

No	R	Binding IC_{50} (μM) (LE)	Functional IC_{50} (μM) (LE)
6		54.9 (0.37)	41.9 (0.38)
10	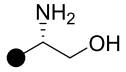	12.8 (0.38)	9.08 (0.39)
11	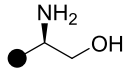	132 (0.30)	241 (0.28)
12	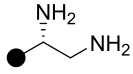	40.1 (0.34)	36.7 (0.34)
13	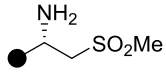	>100	>100
14	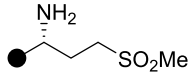	8.97 (0.32)	10.0 (0.32)
15	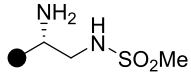	37.9 (0.28)	43.8 (0.28)
16	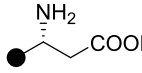	5.69 (0.37)	11.3 (0.35)

behavior in TSA (Figure S2) and that did generate crystals. This protein was used in all subsequent experiments.

A binding assay and a functional assay were used to characterize inhibition by compounds. The binding assay used fluorescence polarization (FP) to measure the displacement of a novel fluorescently labeled hydroxamate compound **5** (see SI) from PaLpxC. This probe resulted from careful optimization of the labeling position and the fluorophore to minimize artifacts from slow binding kinetics probably due to the architecture of the active site of the enzyme. The fluorophore is attached to the sulfone, which occupies the UDP binding pocket and extends out into the solvent. Two different functional assays were used. For the imidazole series, the functional assay measured activity by the reaction of fluorescamine with the free amino group generated on the substrate by LpxC. The glycine series compounds gave interference in the fluorescamine assay, so a liquid chromatography mass spectrometry (LCMS) assay was developed to measure the amount of the product formed. For all assays, compound inhibition or binding is reported as IC_{50} values and ligand efficiency (LE) as $-RT \ln IC_{50}$/heavy atom count.

Hit Identification. The Vernalis fragment library[15,16] of 1152 compounds was screened against PaLpxC using three

https://dx.doi.org/10.1021/acs.jmedchem.0c01215
J. Med. Chem. XXXX, XXX, XXX−XXX

Table 2. Glycine Series: SAR for Extension into the Hydrophobic Tunnel

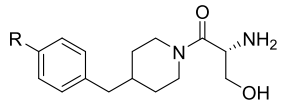

No	17	18	19	20	21
R	H		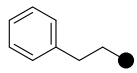	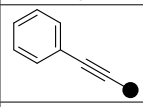	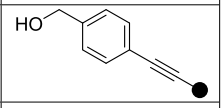
Functional IC_{50} (μM)	24.9	0.660	4.53	0.0340	0.0221
(LE)	(0.34)	(0.35)	(0.28)	(0.39)	(0.37)

ligand-observed NMR experiments (STD, water-LOGSY, and CPMG)[17,18] in pools of six compounds. A binding signal was observed for 252 compounds in one or more NMR experiments. Putative hits were retested as singletons and for competition with either **1** or **4**, chosen to occupy more of the UDP binding pocket (see the modeled structure in Figure S3). Sixteen fragments were competitive with **1** (four of which were positive in all three NMR experiments). Representative hits are shown in Figure 4 (all listed in Table S1). The remaining noncompetitive fragment hits were assessed for competition with **4**, resulting in a further 12 confirmed fragment hits, 4 in all three NMR experiments (structures not shown). These 28 fragment hits were assessed in the FP binding assay. Most bound with lower affinity than the nominal IC_{50} threshold of 2.5 mM, but some showed clear inhibition in the functional assay such as **6** with an IC_{50} of 41.9 μM with a similar IC_{50} in the FP assay.

As shown in Figure 4, crystal structures of representative fragments bound to PaLpxC revealed that molecules that were competitive with the hydroxamate tool compounds in the NMR experiments bound to two sites—coordinated to the zinc (**6**) or in the tunnel (**7**). The tunnel is collapsed somewhat when small zinc-coordinating compounds are bound but expands when compounds are in the tunnel. Some fragments (such as **8**) that are noncompetitive with the hydroxamate tool compounds were found to bind to a site distant from the active site (more than 14 Å through the protein to the zinc ion away from the substrate binding site). This site is preformed in all crystal structures and was also observed in the published crystal structure of **1** (PF-5081090) bound to PaLpxC. The binding site is provided by side chains from several hydrophobic residues (F152 and F176) with F181 at the entrance. Such F181 site compounds were not active in the functional assay and not pursued further.

Two zinc-chelating fragments were selected for investigation, a glycine fragment **6** and an imidazole fragment **9**, both of which were competitive with **1**. In the TSA, **6** and **9** stabilize PaLpxC by 4.0 °C and 0.78 °C, respectively, at 2 mM compound as an additional confirmation of binding.

Fragment to Hit for the Glycine Series. As seen in the crystal structure (Figure 4b), the phenyl ring of the aniline of **6** forms the linker toward the entrance to the tunnel and is sandwiched between hydrophobic amino acid side chains (L18 and A214), while the NH of the aniline makes a water-bridged hydrogen bond to the main chain of M62 (the side chain of this residue is disordered in some of the crystal structures). The zinc-chelating amine group ($N-Zn^{2+}$ distance of ~2.1Å in all glycine series crystal structures) of the amino acid also coordinates to H264 and E77. As expected, modification of that amine group to either dimethylamino, methylamino, hydroxyl, or morpholino led to loss of both binding and enzyme inhibitory activity (data not shown).

We first focused on modification of the amino acid side chain of **6** to optimize interactions in the substrate binding site. Inspection of the crystal structure predicted that the activity would be improved in a D-Ser derivative, which introduces a hydroxyl group to interact with the side chain of T190. This was confirmed in **10** (Table 1 and Figure S4a) with an additional interaction seen in the crystal structure with D241 that also chelates the zinc ion. As predicted, the L-Ser derivative **11** showed a significant decrease in activity; however, the replacement of the hydroxyl of D-Ser with an amino group **12** was less successful. This could be for two reasons. First, the calculated pKa of the chelating NH_2 is reduced from 6.5 in **10** (hydroxyl) to 4.4 in **12** (amino). The pKa is a measure of the strength of bonding of H^+ to the NH_2 of the amino acid; this can be taken as a surrogate for the chelating strength of the NH_2 to the positively charged zinc ion, so a decrease in pKa will mean a decrease in chelating strength.[19] The other reason for the reduction in binding could be due to changes in hydrogen bonding. As shown in Figure S4a, the hydroxyl in **10** donates one hydrogen bond (D241) and accepts one hydrogen bond (T190). Changing the hydroxyl for a positively charged nitrogen (NH_3^+) with three polar hydrogen donors would require T190 to rotate and become an acceptor and still leave one buried unsatisfied hydrogen bond donor.

Modeling from the co-crystallized structure of **10** suggested that a sulfonyl group linked by two carbons but not by one carbon could interact with K238, similar to what is seen for **1**. The increase in potency was confirmed in **14** (compared to **13**) but not improved by replacing the sulfone with a sulfonamide in **15**, perhaps because the chelating ability of the primary amino group was reduced (pKa = 6.2 in **14**, but decreased to pKa = 5.5 in **15**) or perhaps again because of a slight movement of side chains altering the detail of hydrogen bonding. Further modeling suggested that the sulfone could be replaced by a carboxylic acid with a 1-carbon linker to make additional interactions with H264. This carboxylic acid derivative **16** retained potency, and the predicted binding modes of **14** and **16** to PaLpxC were confirmed in crystal structures (Figure S4b,c). However, these modifications

https://dx.doi.org/10.1021/acs.jmedchem.0c01215
J. Med. Chem. XXXX, XXX, XXX−XXX

Table 3. Glycine Series: Antibacterial Activity

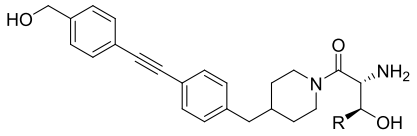

			MIC (μg/mL)			
no.	R	functional IC_{50} (μM)	*E. coli*+ PAβN	*E. coli*[b]	*P. aeruginosa*+ PAβN	*P. aeruginosa*[c]
21	H	0.0221	16	>32	32	>32
22[a]	$CH_2SO_2CH_3$	0.00603	1	64	8	64

[a]Racemic mixture. [b]*Escherichia coli* ATCC25922. [c]*Pseudomonas aeruginosa* ATCC27853.

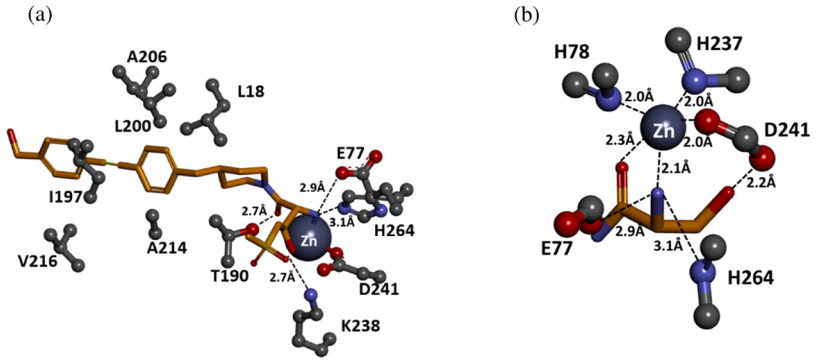

Figure 5. (a). Detail of the crystal structure of **22** binding to the active site of PaLpxC(1-299). See the legend of Figure 3 for conventions used. (b). Different view showing zinc coordination to the selected ligand and protein side-chain atoms showing CD1, NE2, and CD2 of the imidazole of histidines and the carboxylic acid groups of the glutamic and aspartic acids.

Table 4. Imidazole Series: Improving Zinc Chelation[a]

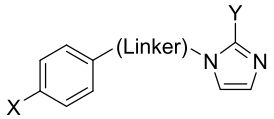

No	X	Linker	Y	Binding IC_{50} (μM) (LE)	Functional IC_{50} (μM) (LE)
9*	H	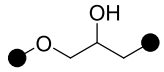	H	>2000 (-)	1130 (0.26)
23*	Cl	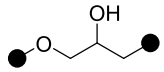	H	259 (0.30)	466 (0.27)
24	Cl	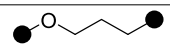	H	118 (0.34)	144 (0.34)
25	Cl	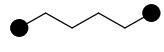	H	43.2 (0.38)	60.4 (0.37)
26	Cl	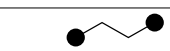	H	2780 (0.26)	Not tested
27	Cl	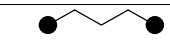	H	125 (0.36)	111 (0.37)
28	Cl	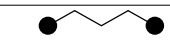	CH_2OH	36.7 (0.37)	108 (0.33)
29*	Cl	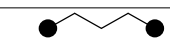	$CH(CH_3)OH$	0.809 (0.47)	10.4 (0.39)

[a]* denotes racemic mixture.

degraded ligand efficiency, so subsequent SAR fixed the D-Ser as the zinc-chelating moiety and explored extension into the hydrophobic tunnel region.

The bound structure of **6** showed limited opportunities for further interactions from the aniline. Replacing the trifluoromethoxy group with extended ethers could not provide a

https://dx.doi.org/10.1021/acs.jmedchem.0c01215
J. Med. Chem. XXXX, XXX, XXX−XXX

good vector into the tunnel region. In addition, the amide NH interacts with the protein only through a water-bridged hydrogen bond. We modeled substituted piperidines and pyrrolidines incorporating additional sp3 carbons to explore the vectors toward the tunnel and also reduce the number of polar H-bond donors. Replacing the aniline with 4-benzyl piperidine (as in **17**) provides a linker with the benzyl group in the entrance of the tunnel with a synthetically accessible vector into the tunnel. Various hydrophobic groups (Table 2) were appended to the para position of the benzyl, which successfully increased potency with retained ligand efficiency. The length and rigidity of the linker between aromatic groups had an effect on activity (as seen comparing **18**, **19**, and **20**), emphasizing the importance of achieving the correct placement in the hydrophobic tunnel.

Introducing an alkyne linker places the second phenyl ring centrally into the hydrophobic tunnel formed by L18, A214, A206, and I197, and addition of a para-hydroxymethyl (in **21**) on this second ring extends into the solvent at the exit of the tunnel. This further improved enzyme activity with some loss of ligand efficiency. Although **21** inhibited the enzyme with an IC_{50} of 20 nM, this did not translate into antibacterial activity (Table 3). Addition of a sulfonyl group (as in **14** to interact with K238) further improved the enzyme activity to single digit nanomolar (**22**). The crystal structure of **22** bound to PaLpxC (Figure 5) confirmed the designed interactions with the protein and the placement of the aromatic rings in the tunnel. The geometry of zinc binding is essentially conserved across the series (Figures S4 and 5b), with a trigonal bipyramidal coordination of the zinc ion, with two oxygens (OD of D241 and ligand carbonyl O) defining the *z*-axis. However, this most potent of the glycine series showed only weak antibacterial activity in the presence of phenylalanine-arginine *β*-naphthylamide (PA*β*N) (an efflux pump inhibitor), so the series was not taken further.

Fragment to Hit for the Imidazole Series. The initial imidazole fragment hit **9** bound weakly to PaLpxC. Exploration of the activity of closely related (near neighbor) compounds established that addition of chlorine to the phenyl moiety (**23**) enhanced activity. The replacement of the hydroxyl by amino or methoxy groups did not lead to improvement (data not shown), but removal of the hydroxyl (**24**) and the oxygen linker (**25**) was beneficial (Table 4) with a much-improved ligand efficiency. Reducing the length of the 4-carbon aliphatic linker between imidazole and chlorophenyl to 2-carbons as in **26** had an impact on activity; 3-carbons retained the same ligand efficiency (**27**), and this was the first imidazole compound to give a crystal structure (Figure S5). This confirmed that the imidazole is a monodentate chelator of the zinc ion, placing the aliphatic chain and chlorophenyl toward the hydrophobic tunnel.

The first optimization was of the imidazole to improve chelation by conversion into a bidentate zinc binder. The crystal structure (Figure S5) suggested that extending from the 2 position of the imidazole would be effective and 2-hydroxymethyl (**28**) retained ligand efficiency, which was further enhanced in **29**, with a 2-(1-hydroxyethyl) group. The co-crystal structure of **29** with PaLpxC (Figure 6) confirmed that the compound forms a bidentate complex with trigonal bipyramidal geometry to the zinc through the hydroxyl oxygen atom and an imidazole nitrogen (see also Figure 8b for details of coordination) to give an optimized hit compound. The structure also suggested that the *S* enantiomer of the 2-(1-hydroxyethyl) group is the most potent.

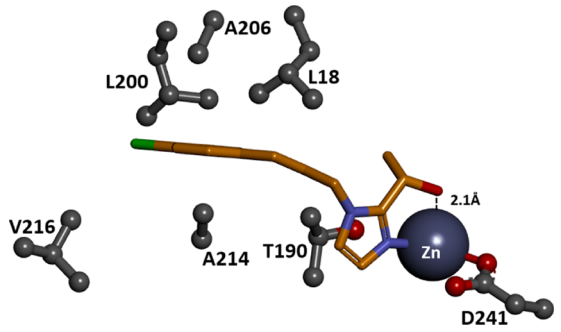

Figure 6. Detail of the crystal structure of **29** binding to the active site of PaLpxC. See the legend of Figure 3 for conventions used.

This exploration of the SAR of the initial imidazole fragment hit illustrates two important features of fragment-based discovery.[20,21] First, the fragment library typically consists of a small number of compounds, selected on physicochemical properties and some measure of chemical diversity.[16] As with any screening approach, the hope is that the library contains something that binds well enough to be characterized. It is then important to optimize the features of the fragment that are making the key interaction with the target binding site, before embarking on large-scale optimization of druglike properties. The second feature is that fragments can provide a diversity of start points for optimization.[22,23] In this study, the zinc-chelating groups of the glycine and imidazole series bind so that the remainder of the compound provides different vectors and opportunities for reaching into the linker and tunnel regions, reflected in the different amino acid groups that are contacted.

Hit to Lead for the Imidazole Series. The co-crystal structure of **29** bound to PaLpxC (Figure 6) suggested how to extend the compound into the hydrophobic tunnel of LpxC with moieties similar to those in the glycine series and other LpxC inhibitors. The exploration of phenyl rings and lengths of a linker (Table 5) showed that, as for the glycine series, the enzyme inhibitory activity tended to improve with elongation of the aromatic portion of the molecule. The ligand efficiency for the placement of a biphenyl moiety into the tunnel was optimal for a 1-carbon (**32**) or a 3-carbon (**34**) rather than a 2-carbon linker (**34**), similar to what is observed for a 2-carbon vs 3-carbon linker to chlorophenyl, comparing **30** to **29** and **31**. This feature was retained with further extension through the hydrophobic tunnel with a Ph-alkyne-Ph moiety (compare **36** with **35** and **37**) with **35** and **37** showing submicromolar functional activity. Although co-crystal structures of this subset of compounds bound to PaLpxC could not be obtained (poor compound behavior), modeling suggested that the variation in the linker length affected the vector between the hydrophobic tunnel binding group and the zinc-chelating groups with a consequent effect on activity. A 1-carbon linker was therefore chosen as optimal for ligand efficiency.

Compound **35** showed weak antibacterial activity against *E. coli* only in the presence of PA*β*N (data not shown). This was probably associated with the high lipophilicity of the compound, and so the next step in optimization was to reduce the lipophilicity by introduction of a heterocycle ring in place of the first phenyl ring attached to the linker.

https://dx.doi.org/10.1021/acs.jmedchem.0c01215
J. Med. Chem. XXXX, XXX, XXX−XXX

Table 5. Imidazole Series: SAR for Extension into the Hydrophobic Tunnel[a]

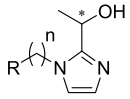

No	R	n	Binding IC_{50} (μM) (LE)	Functional IC_{50} (μM) (LE)
30	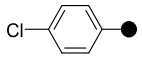	1	39.9 (0.38)	214 (0.32)
31		2	67.8 (0.34)	261 (0.30)
29		3	0.809 (0.47)	10.4 (0.39)
32	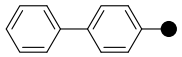	1	0.546 (0.42)	3.94 (0.36)
33		2	6.48 (0.33)	10.4 (0.32)
34		3	0.0269 (0.46)	0.133 (0.42)
35	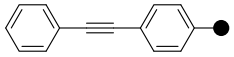	1	0.0929 (0.43)	0.568 (0.38)
36		2	1.76 (0.34)	2.40 (0.33)
37		3	0.0522 (0.41)	0.161 (0.38)
38	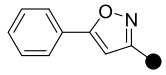	1	0.125 (0.48)	0.884 (0.42)
39	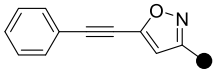	1	0.0206 (0.49)	0.0475 (0.47)

[a]* denotes racemic mixture.

Modeling also suggested that a 5-membered hetero-aromatic ring would favorably adjust the vector between the hydrophobic tunnel and zinc atom binding groups. A number of different heterocycles such as variously substituted 1,3-oxazoles, pyrazoles, triazoles, oxadiazoles, and thiazoles were explored (data not shown), but replacement with a 1,2-oxazole was particularly effective, reducing the cLogP (0.9 for **38** compared to 2.6 for **32**) but also improving the enzyme inhibitor activity by a factor of 4 with a significant improvement in ligand efficiency in both binding and functional assays. This jump in potency can be explained by inspection of the co-crystal structure of **38**, which shows that the five-membered ring creates a turn in the ligand. This change in shape matches the binding site of PaLpxC (Figure 7), and the ligand makes an additional interaction with H19 of the enzyme. The angle and distance to the NE2 atom of H19 are not consistent with a strong hydrogen bond. We noted that the orientation of this histidine does vary between structures depending on the opportunities for alternate hydrogen bonding interactions, notably between H19 and M62 with small adjustments to the main chain conformation.

Compound **39** is a compound with sub-50 nM functional activity, which combines the features learned from the various series to be important for binding, affinity, and antibacterial activity—a 2-(1*S*-hydroxyethyl)imidazole moiety for zinc chelation, 1,2-oxazole for interactions in the linker region, and alkyne to provide a suitable vector to place a phenyl group centrally in the hydrophobic tunnel.

A series of compounds were synthesized based on **39** (Table 6), varying a solubilizing group on the phenyl, which

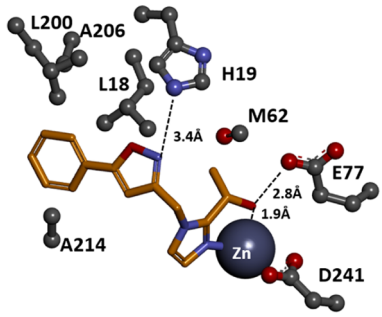

Figure 7. Detail of the crystal structure of **38** binding to the active site of PaLpxC. The carbonyl of M62 is alone; otherwise, see the legend of Figure 3 for conventions used.

as seen in **22** of the glycine series extends through the end of the tunnel into the solvent to give compounds with low nanomolar inhibition of the enzyme activity and with compound properties that provide antibacterial activity.

Analysis of **41** and **42** after chiral separation of the racemic **40** confirmed that the *S* enantiomer is more potent (>100× enzyme inhibition). The *S* enantiomer shows antibacterial activity against a range of Gram-negative bacteria, though the most interesting activity against *P. aeruginosa* is abolished in the presence of human serum albumin (HSA). Further exploration of the solubilizing group produced compounds **44** to **46**, which show similar levels of enzyme inhibition but with more potent antibacterial activity. Compound **46** has the most potent profile of antibacterial activity across a range of bacterial species, but **43** (the structure in Figure 8) shows the least influence of HSA.

Selectivity of Lead Glycine (22) and Imidazole (43) Compounds. Table 7 lists the inhibition measured for the lead compound of each series and a representative hydroxamate compound (BB-78485[24]) against a small panel of matrix metalloprotease enzymes, MMP-2, MMP-3, and MMP-9. The results illustrate that the structure-guided design of each series has generated compounds with selectivity for LpxC over some representative zinc metalloenzymes, in contrast to previously described hydroxamate LpxC inhibitors.

Synthesis of 22 and 43. The synthesis of the advanced compounds **22** and **43** illustrates the general scheme for synthesis of the glycine and imidazole series, respectively. The experimental details are provided in the Experimental Section, and the schemes and synthetic details for all tested compounds are provided in the Supporting Information (SI). These compounds have previously been described in the patents WO 2018/216822, WO 2018/216823, and WO2020/105660. The purity of all compounds was measured by LC, and the identity of compounds was confirmed by MS. The purity of all compounds was > 95%, except for compounds **10** and **15**, which were 92% pure. LC and mass spectrometric traces for the six key compounds **10**, **25**, **29**, **38**, **41**, and **43** are provided in SI.

The synthesis of compound **22** is outlined in Schemes 1 and 2. Scheme 1 shows the synthesis of the amino acid portion of the molecule, intermediate **53**. The Aldol reaction using lithium diisopropylamide and 2-methylsulfanylacetaldehyde gave the intermediate thioether as a racemic mixture of diastereomers **49a** and **49b**. The diastereomers were separated via normal-phase silica gel column chromatography to give the *rac*-(*R**,*R**) diastereomer **49a** and the *rac*-(*R**,*S**)

https://dx.doi.org/10.1021/acs.jmedchem.0c01215
J. Med. Chem. XXXX, XXX, XXX−XXX

Table 6. Imidazole Series: Antibacterial Activity for Various Gram-Negative Bacteria with a variation in the Solubilizing Group[a,b]

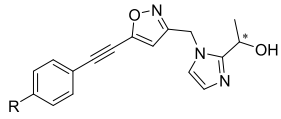

Number	*	R	IC_{50} (nM)[1]	MIC (μg/mL)				
				Ec[2]	*Pa*[3]	*Kp*[4]	*Pa*[5] -HSA	*Pa*[5] + HSA
39	*rac*	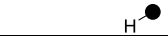	47.5	16	>128	32	64	>128
40	*rac*	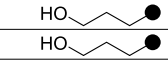	8.96	2	64	4	32	>128
41	*S*		4.03	0.5	32	2	16	>64
42	*R*		1400	>128	>128	>128	>128	>128
43	*S*	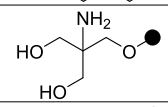	20.0	16	4	64	4	8
44	*S*	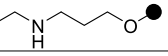	7.04	2	2	32	4	16
45	*S*	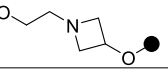	4.42	4	4	4	4	16
46	*S*	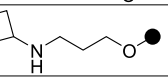	4.63	1	8	1	8	64

[a]*rac* = racemic mixture. [b]1: Functional enzyme activity; 2: *E. coli* ATCC25922; 3: *P. aeruginosa* ATCC27853; 4: *K. pneumoniae* ATCC13883; 5: *P. aeruginosa* 5567.

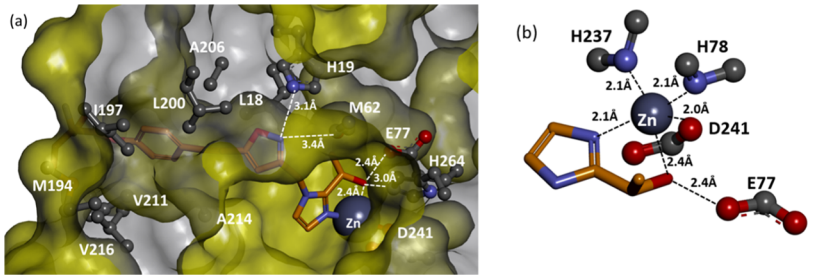

Figure 8. (a) Detail of the crystal structure of **43** binding to the active site of PaLpxC. Clipped, semitransparent solvent accessible surface, yellow outside and gray inside. See the legend of Figure 3 for other conventions used. (b) Different view showing zinc coordination to the selected ligand and protein side-chain atoms as described in the legend to Figure 5(b).

Table 7. Inhibition of MMP Enzymes[a]

compound	MMP-2	MMP-3	MMP-9
22	>100	>100	>100
43	>100	>100	>100
BB-78485	0.0175	0.416	0.0972
Ilomastat (MMP inhibitor)	0.000422	0.0150	0.000177

[a]Values are IC_{50} (μM).

diastereomer **49b** in a 1:1.3 ratio. The relative stereochemistry was determined by X-ray crystallography of ethyl *rac*-(*R**,*S**)-2-(dibenzylamino)-3-hydroxy-4-(methylsulfonyl)-butanoate (**50b**). The *rac*-(*R**,*R**) diastereomer **49a** was subsequently oxidized to the sulfone **50a** using *m*-chloroperbenzoic acid.

Deprotection of the amine by hydrogenation was followed by *tert*-butoxycarbonyl (boc)-protection and hydrolysis of the ethyl ester to afford the intermediate acid **53**. Scheme 2 shows the preparation of the acetylenic portion of the compound and convergent amide coupling with intermediate **53** to make compound **22**. Sonogashira coupling with the triflate **54** (synthesis described in WO 2018/216823) followed by deprotection afforded the intermediate piperidine **56** using HCl in 1,4-dioxane. Amide coupling was performed using HATU, and the final boc-deprotection was facilitated by formic acid.

The synthesis of compound **43** is outlined in Schemes 3−5.

Scheme 3 shows the preparation of intermediate **60** via nucleophilic displacement of the tosylate with 4-iodophenoxide, followed by reduction of the nitro group to the primary amine.

Scheme 4 shows the synthesis of chiral imidazole intermediate **62**. Condensation cyclization of (2*S*)-2-tetrahydropyran-2-yloxypropanal **61** with ammonia and glyoxal afforded the tetrahydropyran-protected intermediate that was subsequently used in the synthesis of several example compounds. Scheme 5 shows the synthesis of compound **43** starting from commercial iodo-1,2-oxazole ester **63**. Sonogashira coupling installed the triisopropylsilyl (TIPS)-protected terminal acetylene group, and a borohydride reduction of the

https://dx.doi.org/10.1021/acs.jmedchem.0c01215
J. Med. Chem. XXXX, XXX, XXX−XXX

Scheme 1. Synthesis of *rac*-(*R,*R**) Acid as the Sodium Salt (53)**[a]

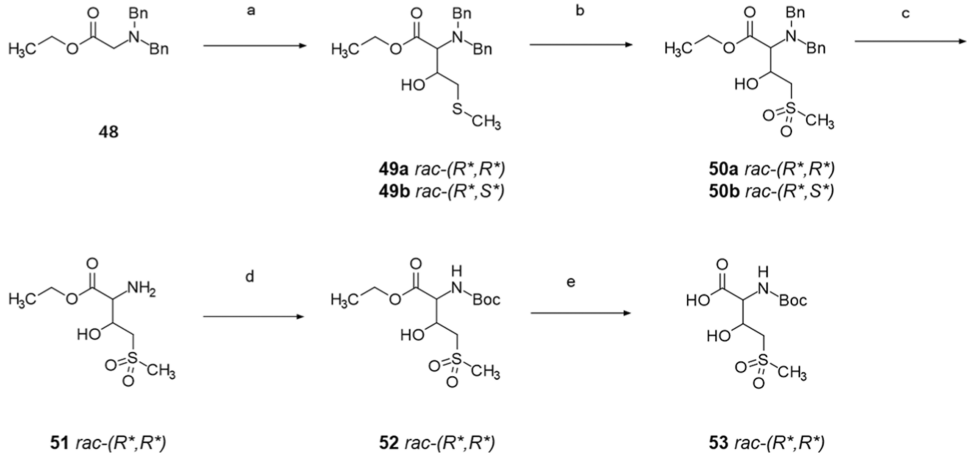

[a]Reagents and conditions: (a) *N*,*N*-diisopropylethylamine (DIPEA), *n*-BuLi, 2-methylsulfanylacetaldehyde, tetrahydrofuran (THF), −78 °C to RT, 30 min, chromatography EtOAc/*n*-hexane, diastereoisomer *rac*-(*R**,*R**) **49a**, 15%, diastereoisomer *rac*-(*R**,*S**) **49b**, 25%; (b) *m*-chloroperbenzoic acid, $CHCl_3$, 0 °C to RT, 16 h, 47%; (c) hydrogen, palladium hydroxide on carbon, EtOH, RT, 16 h, quant; (d) di-*tert*-butyl dicarbonate ($(BOC)_2O$), K_2CO_3, THF, EtOH, RT, 3 h, quant; (e) NaOH (10 M aq), EtOH, RT, 3 h, 73%.

Scheme 2. Synthesis of 2-Amino-3-hydroxy-4-(methanesulfonyl)butan-1-one (22)[a]

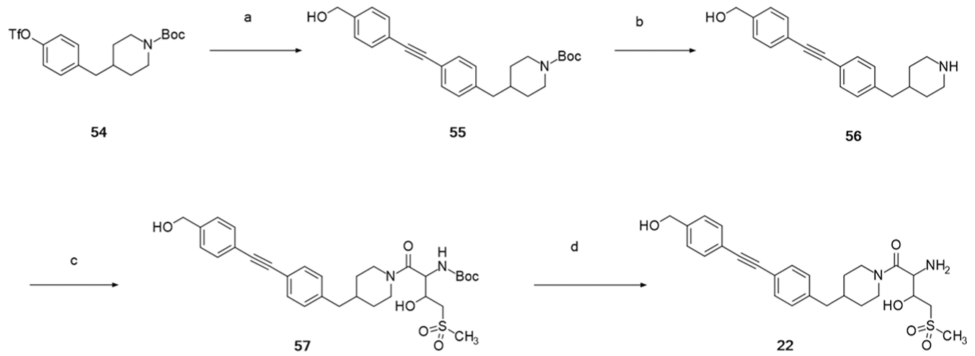

[a]Reagents and conditions: (a) 4-ethynylbenzenemethanol, $PdCl_2(PPh_3)_2$, CuI, triethylamine (TEA), dimethylformamide (DMF), 50 °C, 30 min, 40%; (b) 1,4-dioxane, 4*N* HCl in 1,4-dioxane, RT, 3 h, quant; (c) compound **53**, *O*-(7-azabenzotriazol-1-yl)-*N*,*N*,*N*′,*N*′-tetramethyluronium hexafluorophosphate (HATU), DIPEA, DMF, RT, 3 h, 96%; (d) formic acid, RT, 2 h, 35%.

Scheme 3. Synthesis of Compound 60[a]

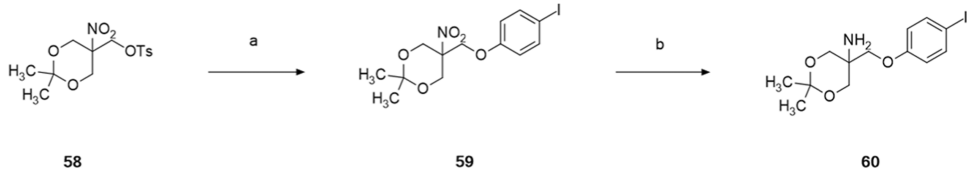

[a]Reagents and conditions: (a) 4-iodophenol, NaH, DMF, 100 °C, 16 h, 75%; (b) iron powder, ammonium chloride, EtOH, Water, 70 °C, 15 h, 88%.

Scheme 4. Synthesis of Imidazole Compound 62[a]

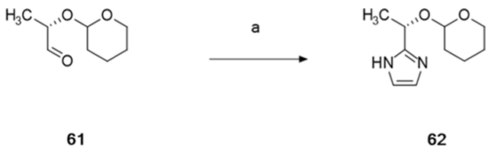

[a]Reagents and conditions: (a) 28% aqueous ammonia, glyoxal, MeOH, RT, 16 h, quant.

ester afforded the intermediate alcohol **65**. The convergent coupling step with imidazole **62** was achieved under Mitsunobu conditions. Following on from deprotection of the TIPS group to form the terminal acetylene using TBAF, a second Sonogashira coupling was performed with compound **60**. The final deprotection of the tetrahydropyranyl (THP)-protected alcohol and acetonide was performed using *p*-toluenesulfonic acid to obtain compound **43**.

CONCLUSIONS

Fragment-based discovery methods have identified two non-hydroxamate series of compounds that are selective inhibitors of the zinc metalloenzyme, LpxC. Optimization of both series was guided by structure-based design to modify zinc

https://dx.doi.org/10.1021/acs.jmedchem.0c01215
J. Med. Chem. XXXX, XXX, XXX−XXX

Scheme 5. Synthesis of Compound 43[a]

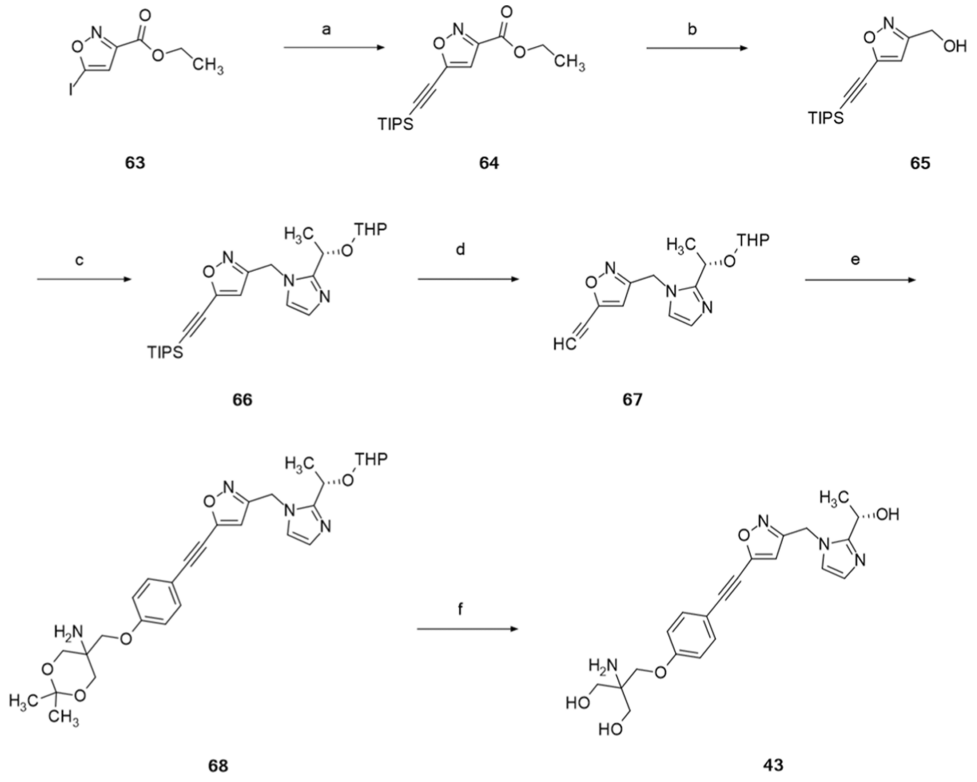

[a]Reagents and conditions: (a) ethynyltri(propan-2-yl)silane, TEA, $Pd(PPh_3)_4$, CuI, DMF, 80 °C, 1 h, 69%; (b) $NaBH_4$, EtOH, 0 °C, 4 h, 89%; (c) **62**, 3-(dimethylcarbamoylimino)-1,1-dimethylurea (TMAD), tributylphosphine, THF, RT, 2 h, 93%; (d) tetra-*n*-butylammonium fluoride (TBAF), THF, 0 °C, 1 h, 82%; (e) **60**, TEA, $PdCl_2(PPh_3)_2$, CuI, DMF, 80 °C, 0.5 h, 55%; (f) *p*-TsOH, MeOH, RT, 1 h, 87%.

chelation, make interactions with the substrate binding cleft, and introduce improved compound properties. The 2-(1*S*-hydroxyethyl)imidazole **43** is an advanced lead compound for which further optimization and *in vivo* efficacy will be described in a future publication.

EXPERIMENTAL SECTION

All chemicals were used directly as received from commercial suppliers. ^1H and ^{13}C NMR spectra were recorded on JNM-ECA600 (600 MHz for ^1H, JEOL), JNM-ECA500 (500 MHz for ^1H and 125 MHz for ^{13}C, JEOL) or AVANCE III HD 400 (400 MHz for ^1H, BRUKER). Chemical shifts for ^1H and ^{13}C NMR are reported in parts per million (ppm) referenced to the residual solvent peak (dimethyl sulfoxide (DMSO)-d_6, δ = 2.50 ppm; $CDCl_3$, δ = 7.27 ppm; CD_3OD, δ = 3.30 ppm). Abbreviations used to describe the peak signals in ^1H NMR data are s = singlet, br = broad, d = doublet, dd = double doublet, dt = double triplet, t = triplet, q = quartet, quin = quintet, m = multiplet. All final compounds were purified to >95% by reverse-phase high-performance liquid chromatography (HPLC) or normal-phase silica gel column chromatography. The purity was assessed by reverse-phase UPLC with a gradient of 5−98% acetonitrile in water (with either an acid or a base modifier) and monitored by UV absorption at 210−450 nm.

Unless otherwise described, the following conditions were used for compound synthesis, purification, and analysis. A microwave synthesizer Initiator$^+$ (Biotage) was used for the microwave reaction conditions. OH-type silica gel column chromatography was performed using SNAP Ultra (Biotage) or REVELERIS 40 μm (Grace), and amino-type silica gel chromatography was performed using SNAP Cartridge ISOLUTE Flash-NH_2 (Biotage) or Grace REVELERIS Amino 40 μm (Grace). The prep-HPLC purifications were performed using Agilent 1260 Infinity or Agilent 6130 (ionization method: electron spray ionization (ESI)), and Agilent 385-ELSD was used when the ELSD detector was attached.

***rac*-(*R**,*R**)-2-Amino-3-hydroxy-1-{4-[(4-{[4-(hydroxymethyl)phenyl] ethynyl}phenyl)methyl]piperidin-1-yl}-4-(methanesulfonyl)butan-1-one (22).** Step 1.

Ethyl *rac*-(*R,*R**)-2-(Dibenzylamino)-3-hydroxy-4-(methylthio)butanoate (49a) and Ethyl *rac*-(*R**,*S**)-2-(Dibenzylamino)-3-hydroxy-4-(methylthio)butanoate (49b).** To a stirred solution of diisopropylamine (4.7 mL, 65 mmol) in THF (0.21 L) was added 1.6 mol/L *n*-butyllithium in hexane (20 mL, 32 mmol) at −78 °C. The mixture was allowed to warm to 0 °C, stirred for 30 min, then cooled to −78 °C, and **48** (6 g, 21 mmol) in THF was added into the mixture. After stirring for 30 min, 2-methylsulfanylacetaldehyde (2.3 g, 25 mmol) in THF was added into the mixture. The reaction mixture was allowed to warm to room temperature, stirred for further 3 h, quenched with a saturated aqueous sodium bicarbonate, and extracted with $CHCl_3$ three times. The organic layer was passed through a phase separator and concentrated in vacuo onto ISOLUTE HM-N. The residue was purified, and diastereomers were separated with OH-type silica gel column chromatography (8−31% EtOAc in *n*-hexane) to afford *rac*-(*R**,*R**) diastereomer (1.2 g, 15% yield) **49a** as yellow oil and *rac*-(*R**,*S**) diastereomer (2.0 g, 25% yield) **49b** as a yellow oil. The relative stereochemistry of both diastereomers was determined by X-ray crystallography of ethyl *rac*-(*R**,*S**)-2-(dibenzylamino)-3-hydroxy-4-(methylsulfonyl)butanoate **49b**. *rac*-(*R**,*R**) diastereomer **49a**: ^1H NMR (400 MHz, $CDCl_3$) δ 7.20−7.35 (m, 10H), 4.24−4.44 (m, 2H), 4.06−4.16 (m, 1H), 3.92 (d, J = 13.57 Hz, 2H), 3.48 (d, J = 13.57 Hz, 2H), 3.30 (d, J = 9.05 Hz, 1H), 3.02 (dd, J = 2.87, 14.12 Hz, 1H), 2.81 (d, J = 3.67 Hz, 1H), 2.30 (dd, J = 9.11, 14.12 Hz, 1H), 2.03 (s, 3H), 1.42 (t, J = 7.15 Hz, 3H). MS (ESI$^+$): m/z 374 $[M + H]^+$. *rac*-(*R**,*S**) diastereomer **49b**: ^1H NMR (400 MHz, $CDCl_3$) δ 7.22−7.39 (m, 10H), 4.22−4.40 (m, 2H), 4.10−4.20 (m, 1H), 4.02 (d, J = 13.20 Hz, 2H), 3.66 (s, 1H), 3.53 (d, J =

https://dx.doi.org/10.1021/acs.jmedchem.0c01215
J. Med. Chem. XXXX, XXX, XXX−XXX

13.20 Hz, 2H), 3.39 (d, J = 9.17 Hz, 1H), 2.63 (dd, J = 2.81, 13.94 Hz, 1H), 2.48 (dd, J = 6.85, 14.06 Hz, 1H), 2.02 (s, 3H), 1.40 (t, J = 7.15 Hz, 3H). MS (ESI^+): m/z 374 $[M + H]^+$.

Ethyl *rac*-(*R,*R**)-2-(Dibenzylamino)-3-hydroxy-4-(methylsulfonyl)butanoate (50a).** To a stirred solution of **49a** (1.2 g, 3 mmol) in $CHCl_3$ (10 mL) was added *m*-chloroperbenzoic acid (2.0 g, 11.6 mmol) at 0 °C. The reaction mixture was stirred at room temperature for 16 h, quenched with a saturated aqueous sodium thiosulfate, and extracted with $CHCl_3$ twice. The organic layer was passed through a phase separator and concentrated in vacuo onto ISOLUTE HM-N. The residue was purified with OH-type silica gel column chromatography (8−100% EtOAc in *n*-hexane) to give the title compound (0.58 g, 47% yield) as a colorless powder. ^1H NMR (400 MHz, $CDCl_3$) δ 7.26−7.40 (m, 10H), 4.58−4.66 (m, 1H), 4.28−4.48 (m, 2H), 3.87 (d, J = 13.08 Hz, 2H), 3.55 (br d, J = 15.04 Hz, 1H), 3.46 (d, J = 12.96 Hz, 2H), 3.21 (d, J = 9.90 Hz, 1H), 3.07−3.15 (m, 1H), 2.93 (s, 3H), 2.62 (dd, J = 10.39, 15.04 Hz, 1H), 1.46 (t, J = 7.15 Hz, 3H). MS (ESI^+): m/z 406 $[M + H]^+$. LCMS condition: C. RT = 0.847 min.

Ethyl *rac*-(*R,*S**)-2-(Dibenzylamino)-3-hydroxy-4-(methylsulfonyl)butanoate (50b).** To a stirred solution of **49b** (0.12 g, 0.32 mmol) in acetonitrile (10 mL) and water (5 mL) was added oxone (0.22 g, 0.35 mmol) at 0 °C. The reaction mixture was stirred at room temperature for 16 h, quenched with a saturated aqueous sodium thiosulfate, and extracted with $CHCl_3$ twice. The organic layer was passed through a phase separator and concentrated in vacuo. The residue was purified with OH-type silica gel column chromatography (0−100% EtOAc in *n*-hexane) to give the title compound (80 mg, 61% yield) as a colorless powder. ^1H NMR (400 MHz, $CDCl_3$) δ 7.24−7.39 (m, 10H), 4.26−4.47 (m, 3H), 4.02 (br d, J = 13.08 Hz, 2H), 3.57 (br d, J = 13.20 Hz, 2H), 3.27−3.41 (m, 1H), 3.09 (dd, J = 8.50, 14.86 Hz, 1H), 2.94−3.02 (m, 1H), 2.91 (s, 3H), 1.42 (t, J = 7.09 Hz, 3H). MS (ESI^+) m/z 406 $[M + H]^+$. X-ray: A single crystal was grown from ethanol. The crystal details were as follows: triclinic space group $P\bar{1}$, a = 11.9376(2) Å, b = 13.4893(3) Å, c = 15.7344(3) Å, α = 69.216(5) °, β = 83.333(6) °; γ = 88.323(6) °; R and wR values were 0.0931 and 0.3597, respectively.

Ethyl *rac*-(*R,*R**)-2-Amino-3-hydroxy-4-(methylsulfonyl)-butanoate (51).** To a solution of **50a** (0.40 g, 1 mmol) in EtOH (9.9 mL) was added 10% palladium hydroxide on carbon (50 mg, catalytic). The mixture was stirred at room temperature for 16 h under a hydrogen atmosphere. The reaction mixture was filtered, and the filtrate was concentrated in vacuo to give crude **51** (0.24 g, quant.) as oil, which was used in the next step without further purification. ^1H NMR (400 MHz, $CDCl_3$) δ 4.41 (ddd, J = 2.14, 5.50, 9.48 Hz, 1H), 4.22−4.29 (m, 1H), 3.72 (q, J = 6.97 Hz, 1H), 3.64 (d, J = 5.50 Hz, 1H), 3.27 (dd, J = 9.90, 15.04 Hz, 1H), 3.19 (br d, J = 14.70 Hz, 1H), 3.04 (s, 3H), 1.32 (t, J = 7.15 Hz, 3H). MS (ESI^+): m/z 226 $[M + H]^+$. LCMS condition: B. RT = 0.258 min.

Ethyl *rac*-(*R,*R**)-2-((*tert*-Butoxycarbonyl)amino)-3-hydroxy-4-(methylsulfonyl) butanoate (52).** To a stirred solution of **51** (0.17 g, 0.75 mmol as the crude material) in THF (3.8 mL) and EtOH (1.5 mL) were added $(BOC)_2O$ (0.20 g, 0.92 mmol) and potassium carbonate (0.27 g, 1.95 mmol). After stirring for 3 h at room temperature, the reaction mixture was quenched with water and extracted with $CHCl_3$ three times. The organic layer was concentrated in vacuo onto ISOLUTE HM-N. The residue was purified with OH-type silica gel column chromatography (30−100% EtOAc in *n*-hexane) to give **52** (0.27 g, quant.) as colorless oil. MS (ESI^+): m/z 348 $[M + Na]^+$. LCMS condition: B. RT = 0.635 min.

Sodium *rac*-(*R,*R**)-2-((*tert*-Butoxycarbonyl)amino)-3-hydroxy-4-(methylsulfonyl) butanoate (53).** To a solution of **52** (0.28 g) in EtOH (2.9 mL) was added 10 mol/L aqueous sodium hydroxide (0.26 mL, 2.6 mmol). After stirring for 3 h at room temperature, the resulting precipitate was collected by filtration and air-dried to afford the title compound (0.20 g, 73% yield) as a colorless solid. MS (ESI^-): m/z 296 $[M - H]^-$. LCMS condition: A. RT = 0.879 min.

***tert*-Butyl 4-(4-((4-(Hydroxymethyl)phenyl)ethynyl)benzyl)-piperidine-1-carboxylate (55).** A mixture of **54** (0.81 g, 1.9 mmol), (4-ethynylphenyl)methanol (0.76 g, 5.7 mmol), CuI (36 mg, 0.19 mmol), $Pd(PPh_3)_2Cl_2$ (0.13 g, 0.19 mmol), and Et_3N (10 mL, 72 mmol) in DMF (10 mL) was stirred under a nitrogen atmosphere at 60 °C for 7 h. After cooling to RT, the mixture was passed through the Celite and washed with EtOAc. The filtrate was concentrated under reduced pressure. The residue was purified with OH-type silica gel chromatography (7−30% EtOAc/*n*-hexane) to give the title compound (0.16 g, 20% yield) as a beige solid. ^1H NMR (400 MHz, $CDCl_3$) δ 7.52 (d, J = 8.07 Hz, 2H), 7.45 (d, J = 8.07 Hz, 2H), 7.35 (d, J = 8.07 Hz, 2H), 7.12 (d, J = 8.07 Hz, 2H), 4.72 (br s, 2H), 3.95−4.18 (m, 2H), 2.58−2.70 (m, 2H), 2.55 (d, J = 6.97 Hz, 2H), 1.58−1.70 (m, 3H), 1.45 (s, 9H), 1.07−1.22 (m, 2H). MS (ESI^+): m/z 428 $[M + Na]^+$. LCMS condition: C. RT = 1.024 min.

(4-((4-(Piperidin-4-ylmethyl)phenyl)ethynyl)phenyl)-methanol Hydrochloride (56). To a solution of **55** (0.14 g, 0.35 mmol) in 1,4-dioxane (4 mL) was added 4 mol/L HCl in 1,4-dioxane (8 mL) at RT. The reaction mixture was stirred at RT for 4 h and concentrated in vacuo to give the title compound (0.13 g, quant.) as a pale-yellow solid.

^1H NMR (400 MHz, DMSO-d_6) δ 7.49 (d, J = 8.07 Hz, 2H), 7.44 (d, J = 8.07 Hz, 2H), 7.36 (d, J = 8.07 Hz, 2H), 7.20 (d, J = 8.07 Hz, 2H), 5.27 (br t, J = 4.58 Hz, 1H), 4.52 (br d, J = 4.28 Hz, 2H), 2.87 (br d, J = 12.23 Hz, 2H), 2.32−2.41 (m, 2H), 1.39−1.62 (m, 3H), 1.03 (dq, J = 3.91, 11.98 Hz, 2H), (two proton signals overlap with the DMSO solvent peak). MS (ESI^+): m/z 306 $[M + H]^+$. LCMS condition: B. Retention time (RT) = 0.543 min.

***rac*-(*R**,*R**)-*tert*-Butyl (3-Hydroxy-1-(4-(4-((4-(hydroxymethyl)phenyl) ethynyl)benzyl)piperidin-1-yl)-4-(methylsulfonyl)-1-oxobutan-2-yl)carbamate (57).** To a stirred solution of **56** (34 mg, 0.1 mmol) in DMF (2.0 mL), **53** (35 mg, 0.11 mmol), HATU (57 mg, 0.15 mmol), and DIPEA (52 μL, 0.54 mmol) were added. The mixture was stirred for 3 h at RT. The reaction mixture was purified via prep-HPLC to give the title compound (56 mg, 96% yield) as an amorphous solid. MS (ESI^+): m/z 607 $[M + Na]^+$. LCMS condition: C. RT = 0.786 min.

***rac*-(*R**,*R**)-2-Amino-3-hydroxy-1-{4-[(4-{[4-(hydroxymethyl)phenyl]ethynyl} phenyl)methyl]piperidin-1-yl}-4-(methanesulfonyl)butan-1-one (22).** A solution of **57** (53 mg, 0.9 mmol) in formic acid (1.5 mL, 40 mmol excess) was stirred for 2 h at RT. The reaction mixture was diluted with $CHCl_3$ and concentrated in vacuo. To the residue was added 7 mol/L ammonia in MeOH (2 mL, excess), and the mixture was stirred for 10 min at RT. The reaction mixture was concentrated in vacuo and purified with prep-HPLC to give the title compound (11 mg, 35% yield) as a colorless powder. ^1H NMR (500 MHz, CD_3OD) δ 7.47 (d, J = 8.23 Hz, 2H), 7.43 (d, J = 7.89 Hz, 2H), 7.36 (d, J = 8.23 Hz, 2H), 7.20 (br d, J = 7.89 Hz, 2H), 4.62 (s, 2H), 4.42−4.57 (m, 3H), 3.92−4.00 (m, 1H), 3.36−3.47 (m, 1H), 3.11−3.23 (m, 1H), 2.94−3.10 (m, 4H), 2.53−2.77 (m, 3H), 1.84−1.98 (m, 1H), 1.75 (br t, J = 12.60 Hz, 2H), 1.09−1.33 (m, 2H). ^{13}C NMR (125 MHz, CD_3OD) δ 163.2, 162.9, 143.4, 142.1, 141.9, 132.6, 132.6, 130.6, 130.5, 128.1, 123.7, 123.6, 122.6, 122.5, 90.1, 90.0, 66.4, 66.4, 64.9, 57.1, 57.0, 56.7, 47.4, 47.2, 44.2, 43.6, 43.4, 43.3, 39.2, 39.0, 33.7, 33.7, 33.0, 32.8, 31.1 (35 carbon signals are observed because of the rotational isomer). MS (ESI^+): m/z 485 $[M + H]^+$. high-resolution mass spectrometry (HRMS) (ESI^+/APCI) calcd. for $[C_{26}H_{32}N_2O_5S + H]^+$: 485.2105; found: 485.2089. LCMS condition: B. RT = 0.590 min.

2-Amino-2-[(4-{[3-({2-[(1*S*)-1-hydroxyethyl]-1*H*-imidazol-1-yl}methyl)-1,2-oxazol-5-yl]ethynyl}phenoxy)methyl]propane-1,3-diol (43). Step 1.

5-[(4-Iodophenoxy)methyl]-2,2-dimethyl-5-nitro-1,3-dioxane (59). To a solution of 4-iodophenol (2.1 g, 9.6 mmol) in DMF (96 mL) was added NaH (0.50 g, 12 mmol) and stirred for 1.5 h at room temperature. To the reaction mixture was added **58** (3.6 g, 11 mmol) and stirred for an additional 16 h at 100 °C. The resulting mixture was diluted with EtOAc and washed with water. The organic layer was dried over $MgSO_4$ and concentrated in vacuo. The

https://dx.doi.org/10.1021/acs.jmedchem.0c01215
J. Med. Chem. XXXX, XXX, XXX−XXX

residue was triturated with diethyl ether and collected by filtration to afford the title compound (2.8 g, 75% yield) as a colorless solid. ^{1}H NMR (400 MHz, $CDCl_3$) δ 7.57 (d, J = 8.93 Hz, 2H), 6.67 (d, J = 8.93 Hz, 2H), 4.45 (d, J = 12.72 Hz, 2H), 4.42 (s, 2H), 4.15 (d, J = 12.59 Hz, 2H), 1.46 (s, 3H), 1.43 (s, 3H).

5-[(4-Iodophenoxy)methyl]-2,2-dimethyl-1,3-dioxan-5-amine (60). To a solution of **59** (0.20 g, 0.51 mmol) in EtOH (2.0 mL) and water (1.0 mL) were added ammonium chloride (41 mg, 0.77 mmol) and iron powder (0.17 g, 3.1 mmol). After being stirred for 15 h at 70 °C, the reaction mixture was filtered through Celite. The filtrate was concentrated in vacuo. The residue was diluted with EtOAc and washed with saturated sodium bicarbonate. The organic layer was dried over $MgSO_4$ and concentrated in vacuo. The residue was purified with amino-type silica gel column chromatography (10−40% EtOAc in *n*-hexane) to afford the title compound (0.16 g, 88% yield) as a colorless solid. ^{1}H NMR (400 MHz, $CDCl_3$) δ 7.56 (d, J = 8.80 Hz, 2H), 6.71 (d, J = 8.80 Hz, 2H), 3.96 (s, 2H), 3.89 (d, J = 11.62 Hz, 2H), 3.63 (d, J = 11.62 Hz, 2H), 1.47 (s, 3H), 1.42 (s, 3H).

Ethyl 5-{[Tri(propan-2-yl)silyl]ethynyl}-1,2-oxazole-3-carboxylate (64). A round−bottomed flask was charged with **63** (18 g, 67 mmol), ethynyltri(propan-2-yl)silane (12 g, 67 mmol), DMF (52 mL), and TEA (73 mL, 1 mol, in excess). The flask was evacuated and backfilled with nitrogen, followed by addition of $Pd(PPh_3)_4$ (2.4 g, 2 mmol) and CuI (0.80 g, 4.2 mmol). After being stirred for 1 h at 80 °C, the mixture was poured into a half-saturated aqueous ammonium chloride and extracted three times with EtOAc-hexane (1:1). The combined organic layer was washed with water, dried over $MgSO_4$, and concentrated in vacuo. The residue was purified with OH-type silica gel column chromatography (0−15% EtOAc in *n*-hexane) to give the title compound (12 g, 69% yield) as a pale-yellow oil. ^{1}H NMR (400 MHz, $CDCl_3$) δ 6.81 (s, 1H), 4.45 (q, J = 7.1 Hz, 2H), 1.42 (t, J = 7.1 Hz, 3H), 1.09−1.23 (m, 21H). MS (ESI$^+$/APCI): m/z 322 $[M + H]^+$.

(5-{[Tri(propan-2-yl)silyl]ethynyl}-1,2-oxazol-3-yl)methanol (65). To a cooled (0 °C) solution of **64** (10 g, 32 mmol) in EtOH (53 mL) and THF (103 mL) was added $NaBH_4$ (2.4 g, 64 mmol) in portions while keeping the internal temperature below 5 °C. After stirring for 3 h at 0 °C, half-saturated aqueous ammonium chloride was added to the reaction mixture while keeping the internal temperature below 15 °C. The mixture was stirred for 30 min at room temperature and concentrated under reduced pressure, and the resulting aqueous solution was extracted three times with $CHCl_3$. The combined organic layer was washed with brine, dried over $MgSO_4$, and concentrated in vacuo. The residue was purified with OH-type silica gel column chromatography (10−50% EtOAc in *n*-hexane) to give the title compound (7.9 g, 89% yield) as a pale-yellow oil. ^{1}H NMR (400 MHz, $CDCl_3$) δ 6.49 (s, 1H), 4.77 (s, 2H), 1.02−1.25 (m, 21H). MS (ESI$^+$): m/z 280 $[M + H]^+$. LCMS condition: C. RT = 1.078 min.

3-[(2-{(1*S*)-1-[(Oxan-2-yl)oxy]ethyl}-1*H*-imidazol-1-yl)methyl]-5-{[tri(propan-2-yl)silyl]ethynyl}-1,2-oxazole (66). To a stirred solution of **65** (1.4 g, 4.8 mmol) and **62** (1.1 g, 5.8 mmol) in THF (19 mL) were added TMAD (1.1 g, 6.3 mmol) and tributylphosphine (1.3 mL, 6.3 mmol) at 0 °C under a nitrogen atmosphere, and the mixture was stirred for 3.5 h at RT. The reaction mixture was quenched by water and extracted three times with EtOAc. The organic layer was dried over $MgSO_4$ and concentrated in vacuo onto ISOLUTE HM-N. The residue was purified with OH-type silica gel column chromatography (40−80% EtOAc in *n*-hexane) to afford the title compound **66** (1.5 g, 68% yield) as a yellow oil. ^{1}H NMR (600 MHz, $CDCl_3$) δ 6.85−7.08 (m, 2H), 6.16−6.35 (m, 1H), 5.29−5.50 (m, 2H), 5.06−5.19 (m, 1H), 4.46−4.75 (m, 1H), 3.81−3.95 (m, 1H), 3.42−3.56 (m, 1H), 1.05−1.85 (m, 30H). MS (ESI$^+$): m/z 458 $[M + H]^+$. LCMS condition: B. RT = 1.096 min.

5-Ethynyl-3-[(2-{(1*S*)-1-[(oxan-2-yl)oxy]ethyl}-1*H*-imidazol-1-yl)methyl]-1,2-oxazole (67). To a cooled (0 °C) solution of **66** (12 g, 26 mmol) in THF (0.18 L) was added TBAF (28 mL, 1 mol/L solution in THF), while the internal temperature was maintained below 5 °C. After stirring for 1 h at 0 °C, the mixture was concentrated, and the residue was diluted with EtOAc followed by washing with water and brine. The organic phase was separated, dried over $MgSO_4$, and concentrated under reduced pressure. The residue was purified with OH-type silica gel column chromatography (50−100% EtOAc in n-hexane and then 0−10% MeOH in EtOAc) to give the title compound (6.5 g, 82% yield) as a brown oil. ^{1}H NMR (400 MHz, $CDCl_3$) δ 6.99−7.05 (m, 1H), 6.87 (br s, 1H), 6.25−6.40 (m, 1H), 5.31−5.51 (m, 2H), 3.81−3.98 (m, 1H), 5.06−5.15 (m, 1H), 4.46−4.75 (m, 1H), 3.61−3.65 (m, 1H), 3.42−3.55 (m, 1H), 1.70−1.84 (m, 1H), 1.37−1.66 (m, 8H). MS (ESI$^+$): m/z 302$[M + H]^+$. LCMS condition: B. RT = 0.415 min.

2,2-Dimethyl-5-[[4-[2-[3-[[2-[(1*S*)-1-tetrahydropyran-2-yloxyethyl]imidazol-1-yl]methyl]isoxazol-5-yl]ethynyl]-phenoxy]methyl]-1,3-dioxan-5-amine (68). A round-bottomed flask was charged with **67** (110 mg, 0.37 mmol), **60** (110 mg, 0.3 mmol), $PdCl_2(PPh_3)_2$ (11 mg, 0.015 mmol), and CuI (5.8 mg, 0.03 mmol). The flask was evacuated and backfilled with nitrogen followed by addition of DMF (3.0 mL) and TEA (0.52 mL, 0.7 mmol). The mixture was placed into a preheated oil bath (50 °C) and stirred for 30 min. The reaction mixture was diluted with $CHCl_3$, followed by washing with 10% aqueous ammonium hydroxide and brine. The organic phase was separated, dried over $MgSO_4$, and concentrated under reduced pressure. The residue was purified with amino-type silica gel chromatography (20−100% EtOAc in *n*-hexane) to afford the title compound (90 mg, 55% yield) as a yellow oil. ^{1}H NMR (400 MHz, $CDCl_3$) δ 7.46−7.54 (m, 2H), 6.99−7.08 (m, 1H), 6.88−6.98 (m, 3H), 6.19−6.34 (m, 1H), 5.32−5.49 (m, 2H), 5.13 (quin, J = 6.85 Hz, 1H), 4.47−4.77 (m, 1H), 4.04 (s, 2H), 3.43−3.95 (m, 6H), 1.37−1.89 (m, 15H). MS (ESI$^+$): m/z 537 $[M + H]^+$. LCMS condition: A. RT = 0.835 min.

2-Amino-2-[(4-{[3-({2-[(1*S*)-1-hydroxyethyl]-1*H*-imidazol-1-yl}methyl)-1,2-oxazol-5-yl]ethynyl}phenoxy)methyl]propane-1,3-diol (43). To a solution of **68** (0.11 g, 0.20 mmol) in MeOH (2.0 mL) and water (0.20 mL) was added p-TsOH monohydrate (91 mg, 0.48 mmol) at RT. After being stirred for 20 h, the reaction mixture was basified with saturated aqueous sodium bicarbonate at 0 °C and extracted with chloroform. The organics were combined and passed through a phase separator and concentrated in vacuo. The residue was purified with amino-type silica gel chromatography (10% MeOH in chloroform) to give the title compound (61 mg, 75% yield) as a colorless amorphous solid.

^{1}H NMR (500 MHz, DMSO-d_6) δ 7.57 (d, J = 9.17 Hz, 2H), 7.16 (d, J = 1.15 Hz, 1H), 7.03 (d, J = 8.79 Hz, 2H), 6.81 (d, J = 1.15 Hz, 1H), 6.79 (s, 1H), 5.38−5.47 (m, 3H), 4.85 (quin, J = 6.40 Hz, 1H), 4.61 (br s, 2H), 3.82 (s, 2H), 3.33−3.40 (m, 2H), 1.46 (d, J = 6.88 Hz, 3H).

^{13}C NMR (125 MHz, DMSO-d_6) δ 161.6, 160.6, 152.9, 149.7, 133.6, 126.5, 120.9, 115.2, 111.1, 107.5, 99.0, 74.1, 69.6, 63.0, 61.4, 56.4, 40.5, 21.8. HRMS (ESI$^+$/APCI) calcd for $[C_{21}H_{24}N_4O_5 + H]^+$: 413.1819; found: 413.1800.

General Experimental Details for Assays and Structure Determination. UDP-3-*O*-(*R*-3-hydroxydecanoyl)-*N*-acetylglucosamine was obtained from Alberta Research Council (Alberta, Canada) and stored as 100mM stock dissolved in DMSO at −80 °C.

Fluorescamine was obtained from FUJIFILM Wako Pure Chemical Corporation or Sigma-Aldrich.

Uridine diphosphate *N*-acetylglucosamine (UDP-GlcNAc) was stored as 200 μM stock dissolved in methanol−acetonitrile (1:1) at −20 °C.

Compounds were stored as 10 mM, 20 mM, 50 mM, or 200 mM stock in DMSO.

Protein Production. PaLpxC(1-299)C40S. Plasmids encoding P. aeruginosa LpxC(1-299) with a mutation, C40S, were obtained from ATUM, in the T7 expression vector pJ411 (ATUM).

MIKQRTLKNIIRATGVGLHSGEKVYLTLKPAPVDT-GIVFSRTDLDPVVEIPARAENVGETTMSTTLVKGDVKVDT-VEHLLSAMAGLGIDNAYVELSASEVPIMDGSAGPFVFLIQSAGL-

https://dx.doi.org/10.1021/acs.jmedchem.0c01215
J. Med. Chem. XXXX, XXX, XXX−XXX

QEQEAAKKFIRIKREVSVEEGDKRAVFVPFDGFKVS-FEIDFDHPVFRGRTQQASVDFSSTSFVKEVSRARTFGFMR-DIEYLRSQNLALGGSVENAIVVDENRVLNEDGLRYEDEFVKH-KILDAIGDLYLLGNSLIGEFRGFKSGHALNNQLLRTLIADKDA-WEVVTFEDARTAPISYMRP

Plasmids were transformed into *E. coli* BL21(DE3) pLysS cells. Cultures were grown at 37 °C in Terrific Broth with Kanamycin (100 μg/mL) until the OD_{600} was 0.7 at which time the temperature was reduced to 30 °C and expression induced by addition of isopropyl β-D-1-thiogalactopyranoside (IPTG) to a final concentration of 1 mM in the presence of 0.1 mM $ZnCl_2$ or $ZnSO_4$. Cells were harvested by centrifugation after 2 h.

For ^{15}N-labeled PaLpxC, the transformed cells were grown in EnpressoB, Nitrogen Free (Enpresso), supplemented with 2.5 g/L ^{15}N-$(NH_4)_2SO_4$ (Goss Scientific) induced as above and harvested after 3 h.

Cells were resuspended in 3 volumes of 20 mM 4-(2-hydroxyethyl)-1-piperazineethanesulfonic acid (HEPES) (pH 7.0) and 2 mM DTT and lysed by passing three times through a Stanstead Homogenizer (Stanstead). The lysate was clarified by centrifugation and applied to CaptoQ, eluting in a gradient to 1 M NaCl. $(NH_4)_2SO_4$ was added to a final concentration of 1 M, and the LpxC was further purified by hydrophobic interaction chromatography using HiTrap Butyl HP (GE Healthcare) with a gradient of 1−0 M $(NH_4)_2SO_4$ and finally Superdex200pg (GE Healthcare), equilibrated in 20 mM HEPES (pH 7.4), 150 mM NaCl, and 2 mM DTT.

PaLpxC(1-303-His). The gene fragment encoding residues 2-303 of PaLpxC was amplified using primers with NdeI and NotI sites and subcloned into pET21a vectors. The protein was expressed in *E. coli* BL21(DE3)pLysS cells by inducing with 1.0 mM IPTG and 0.2 mM $ZnSO_4$ at OD_{600} = 0.5 for 7 h at 18 °C. The protein was purified using TALON metal affinity resin (TaKaRa) and buffer-exchanged against 40 mM HEPES (pH 8.0) using PD-10 (GE Healthcare).

TSA Methods. Fluorescence was measured on an Agilent MX300P Real-Time PCR with a heating rate of 1 °C per minute and Ex/Em 492/610 nm. Final concentrations used were 5 μM PaLpxC, 5× Sypro Orange, 40 mM HEPES (pH 8.0), and 2% DMSO in a final volume of 40 μL. Protein denaturation curves were measured in the absence and presence of low nM affinity compounds **1** (PF-5081090), which were added at a 10-fold excess of the protein concentration.

When evaluating compounds, fluorescence was measured on an Applied Biosystems 7500 Fast Real-Time PCR system with a heating rate of 0.96 °C per minute (ramp rate: 1%) and the ROX (carboxy-X-rhodamine) detector. Final concentrations used were 5 μM PaLpxC(1-303-His), 1× Protein Thermal Shift Dye (Life Technologies), 40 mM HEPES (pH 8.0), 10 or 40 μM $ZnCl_2$, and 5% DMSO in a final volume of 20 μL. Protein denaturation curves were measured in the absence and presence of compounds which were added at a more than 10-fold excess of the protein concentration.

Crystallization and Structure Determination by X-ray Crystallography. Co-Crystallization to Establish Initial Crystals. PaLpxC at 10.6 mg/mL was mixed with compound **47** (see SI) at 4-fold molar excess. The complex crystallized in 0.1 M Tris (pH 8.5), 30% poly(ethylene glycol) 4 K, and 0.2 M $MgCl_2$ using the sitting-drop vapor-diffusion method at 19 °C. The co-crystals took 2 weeks to grow. The compound binds in the tunnel region, making no contact with zinc.

*Protein−Ligand Complexes Containing **4**, **5**, and **24**.* Co-crystals containing **47** were soaked out and compounds 4, 5, or 24 subsequently soaked in, also overnight. The protein crystals were flash-frozen at 100 K using a cryo-protection buffer consisting of mother liquor with 20−25% glycerol added.

Protein−Ligand Complexes Containing Other Compounds. Details of the conditions under which crystals were obtained by co-crystallization of individual compounds are in SI.

Data Collection. Diffraction data of both the soaked and co-crystals were collected at 100 K at either Diamond Light Source (UK), Soleil Synchrotron (France), in-house on a Bruker D8 Venture TXS Generator with a Bruker Photon 100 detector, or in-house on a Micro Max 007 HF Generator (Rigaku) with an R-AXIS VII detector (Rigaku) or PILATUS 200K (Rigaku). Data processing was carried out with XDS[25], SAINT and SADABS (Bruker AXS Inc., Madison, Wisconsin), CrystalClear (Rigaku) or CrysAlisPro (Rigaku). Data collection statistics are summarized in Table S2.

Structure Determination. Crystallographic data was processed and structures determined and refined within the CCP4 package[26] using Sketcher (CCP4) or ProDrg[27] to build models of each compound. The structures were determined by molecular replacement using the published structure (PDBcode 3UHM) to calculate model phases and subsequently refined using REFMAC5.[28] Interactive graphical model building was carried out with COOT.[29] In all structures, the respective ligands were clearly defined by the initial electron density maps; Table S2 includes an image of the 2Fo-Fc map around each ligand.

NMR Methods. All protein NMR spectra were recorded on a 600 MHz Bruker Avance III spectrometer fitted with a cryoprobe.

$^1H-^{15}N$ HSQC NMR spectra were recorded with ^{15}N-labeled PaLpxC at 250 μM in 20 mM HEPES (pH 7.4), 150 mM NaCl, and 5% D_2O.

Ligand-observed fragment screening was performed with 500 μM of each compound, 10 μM PaLpxC in 20 mM HEPES (pH 7.4) and, 15 μM NaCl, in mixtures of six compounds per sample as described previously.[17,18]

Computational Methods. Compounds and proteins were modeled using the Schrödinger Suite of programs (mmshare-v32018:mmshare-v3.5, Schrödinger, LLC, New York, NY). Protein structure preparation (PrepWizard), ligand preparation (Ligprep), and generation of docking grids were run with defaults. Docking was carried out using Glide, with and without constraints in the positions of the atoms chelating the zinc.

Calculations of pKa were performed with the ACD/Percepta software (ACD/Labs 2017.13, Advanced Chemistry Development, Inc) packaged in Classic mode, not using GALAS.

Fluorescence Polarization (FP) Assay. Compounds were screened in a 50 μL assay containing 20 nM PaLpxC or PaLpxC(1-303-His), 5 nM fluorescein probe **5**, 40 mM HEPES (pH 7.5), 150 mM NaCl, 0.02% Tween 20, with or without 25 nM $ZnCl_2$, and 5% DMSO. PaLpxC and compounds were preincubated for 30 minutes prior to addition of the fluorescein probe, and the assay was then incubated for a further 2 h at room temperature. Plates were read on either a Biotek Synergy Neo Plate reader Ex/Em 485(20)/528(20) nm, Envision 2101 (Ex/Em 480/535 nm), or PHERAStar FSX (Ex/Em 485/535 nm) in conjunction with polarizing filters.

Inhibition values were calculated from control DMSO samples containing no compound (0% inhibition) and samples containing no enzyme (100% inhibition). Data reported in the tables is the geometric mean of at least two determinations; compound **69** or BB-78485[24] was included in assays as a control with IC_{50} values in the range 0.10−0.40 and 0.015−0.060 μM, respectively. The synthesis of **69** is described in the Supporting Information.

Fluorescamine-Based Functional Activity Assay. Imidazole series compounds were assayed with 3.6 nM PaLpxC(1-303-His), 20 μM UDP-3-*O*-(*R*-3-hydroxydecanoyl)-*N*-acetylglucosamine (substrate), 40 mM HEPES (pH 8.0), 25 nM $ZnCl_2$, 0.02% Brij-35, and 5% DMSO. Assay plates were incubated for 60 min at room temperature and terminated by the addition of 1.0 mg/mL fluorescamine in 1:1 dimethylformamide/acetonitrile followed by 0.2 M sodium phosphate buffer (pH 8.0) and incubated. Plates were read on an Enspire: Ex/Em 390/495 nm.

Inhibition values were calculated from control DMSO samples containing no compound (0% inhibition) and samples containing no PaLpxC(1-303-His) (100% inhibition); compound **69** or BB-78485[24] was included in assays with IC_{50} values in the range

https://dx.doi.org/10.1021/acs.jmedchem.0c01215
J. Med. Chem. XXXX, XXX, XXX−XXX

0.30−1.2 and 0.010−0.040 μM, respectively. Data reported in tables are the geometric mean of at least two determinations.

This assay measures the extent to which LpxC catalyzes the removal of the acetyl group from the acetylglucosamine by the reaction of the resulting free amino group with fluorescamine. It is therefore not suitable for the glycine series.

Matrix Metalloprotease (MMP) Assays. The MMP inhibitor profiling kit, Fluorometric RED (Enzo Life Sciences, Inc., Farmingdale, NY), was used for the human MMP inhibition assays. The inhibitory activities of compounds against MMP-2, 3, and 9 were evaluated as described in the kit protocol with some modifications. In brief the assay volume was modified to 50 μL and final enzyme concentrations of MMP-2, 3, and 9 were modified to 18.3, 21.0, and 5.67 mU/μL, respectively. Fluorescence (Ex/Em 545/576 nm) was detected using the CLARIOstar (BMG Labtech). Ilomastat (GM-6001)[30] is an MMP inhibitor used as a positive control. Values reported are the geometric mean of two determinations.

Mass-Spectrometry-Based Functional Activity Assay. Glycine series compounds were screened with 3.6 nM PaLpxC(1-303-His), 20 μM UDP-3-*O*-(*R*-3-hydroxydecanoyl)-*N*-acetylglucosamine (substrate), 40 mM HEPES (pH 8.0), 25 nM $ZnCl_2$, 0.02% Brij-35, and 5% DMSO. Samples were incubated for 60 min at room temperature, and the reaction was terminated by the addition of four times the volume of acetonitrile containing 25 μM UDP-GlcNAc as the internal standard. The mixture was centrifuged, and the supernatant was injected into liquid chromatography-tandem mass spectrometry (LC/MS/MS). The samples were separated with Inertsil Amide (3.0 μm, 50 mm × 2.1 mm I.D., GLScience, Japan) with a Shimadzu HPLC system. The mobile phase was 8 mM ammonium acetate containing 72% acetonitrile, and the flow rate was 0.2 mL/min. MS/MS detection of each component (*m*/*z* 734 and *m*/*z* 385) was performed using a TSQ Quantum system (Thermo Fisher Scientific) or a QTRAP-5500 system (Sciex) with the electrospray interface in negative ion detection mode.

Inhibition values were calculated from product signals of control DMSO samples containing no compound (0% inhibition) and samples containing no substrate (100% inhibition). The control compound **69** was included in assays with IC_{50} values in the range of 0.25−1.0 μM. Data reported in tables are the geometric mean of at least two determinations.

Evaluation of Antibacterial Activity. The minimum inhibitory concentration (MIC) was determined using the Clinical and Laboratory Standards Institute (CLSI) methodology, described in a CLSI document.[31] *P. aeruginosa* 5567 was a clinical isolate obtained in Japan. Where used, the PAβN concentration was 50 μg/mL for *P. aeruginosa* and 200 μg/mL for *E. coli*; the HSA concentration was 5% w/v.

■ ASSOCIATED CONTENT

Supporting Information

The Supporting Information is available free of charge at https://pubs.acs.org/doi/10.1021/acs.jmedchem.0c01215.

Synthesis of compounds **9**−**24** and **26**−**32**; structural biology data (PDF)

Molecular formula strings (CSV)

Accession Codes

The refined coordinates of the structures presented in this manuscript are deposited at the RCSB with the following codes: **6**: 7CIC, **7**: 7CIB, **8**: 7CIA, **10**: 7CIE, **14**: 7CI4, **16**: 7CI5, **22**: 7CI7, **27**: 7CID, **29**: 7CI6, **38**: 7CI8, and **43**: 7CI9. The authors will release the atomic coordinates and experimental data upon article publication

■ AUTHOR INFORMATION

Corresponding Authors

Yousuke Yamada − *Taisho Pharmaceutical Co., Ltd., Saitama 331-9530, Japan*; Email: yo-yamada@taisho.co.jp

Roderick E. Hubbard − *Vernalis (R&D) Ltd., Cambridge CB21 6GB, U.K.*; Email: r.hubbard@vernalis.com

Authors

Hajime Takashima − *Taisho Pharmaceutical Co., Ltd., Saitama 331-9530, Japan*

David Lee Walmsley − *Vernalis (R&D) Ltd., Cambridge CB21 6GB, U.K.*

Fumihito Ushiyama − *Taisho Pharmaceutical Co., Ltd., Saitama 331-9530, Japan*

Yohei Matsuda − *Taisho Pharmaceutical Co., Ltd., Saitama 331-9530, Japan*

Harumi Kanazawa − *Taisho Pharmaceutical Co., Ltd., Saitama 331-9530, Japan*

Toru Yamaguchi-Sasaki − *Taisho Pharmaceutical Co., Ltd., Saitama 331-9530, Japan*

Nozomi Tanaka-Yamamoto − *Taisho Pharmaceutical Co., Ltd., Saitama 331-9530, Japan*

Junya Yamagishi − *Taisho Pharmaceutical Co., Ltd., Saitama 331-9530, Japan*

Risa Kurimoto-Tsuruta − *Taisho Pharmaceutical Co., Ltd., Saitama 331-9530, Japan*

Yuya Ogata − *Taisho Pharmaceutical Co., Ltd., Saitama 331-9530, Japan*

Norikazu Ohtake − *Taisho Pharmaceutical Co., Ltd., Saitama 331-9530, Japan*

Hayley Angove − *Vernalis (R&D) Ltd., Cambridge CB21 6GB, U.K.*

Lisa Baker − *Vernalis (R&D) Ltd., Cambridge CB21 6GB, U.K.*

Richard Harris − *Vernalis (R&D) Ltd., Cambridge CB21 6GB, U.K.*

Alba Macias − *Vernalis (R&D) Ltd., Cambridge CB21 6GB, U.K.*

Alan Robertson − *Vernalis (R&D) Ltd., Cambridge CB21 6GB, U.K.*

Allan Surgenor − *Vernalis (R&D) Ltd., Cambridge CB21 6GB, U.K.*

Hayato Watanabe − *Taisho Pharmaceutical Co., Ltd., Saitama 331-9530, Japan*

Koichiro Nakano − *Taisho Pharmaceutical Co., Ltd., Saitama 331-9530, Japan*

Masashi Mima − *Taisho Pharmaceutical Co., Ltd., Saitama 331-9530, Japan*

Kunihiko Iwamoto − *Taisho Pharmaceutical Co., Ltd., Saitama 331-9530, Japan*

Atsushi Okada − *Taisho Pharmaceutical Co., Ltd., Saitama 331-9530, Japan*

Iichiro Takata − *Taisho Pharmaceutical Co., Ltd., Saitama 331-9530, Japan*

Kosuke Hitaka − *Taisho Pharmaceutical Co., Ltd., Saitama 331-9530, Japan*

Akihiro Tanaka − *Taisho Pharmaceutical Co., Ltd., Saitama 331-9530, Japan*

Kiyoko Fujita − *Taisho Pharmaceutical Co., Ltd., Saitama 331-9530, Japan*

Hiroyuki Sugiyama − *Taisho Pharmaceutical Co., Ltd., Saitama 331-9530, Japan*

Complete contact information is available at: https://pubs.acs.org/10.1021/acs.jmedchem.0c01215

https://dx.doi.org/10.1021/acs.jmedchem.0c01215
J. Med. Chem. XXXX, XXX, XXX−XXX

Author Contributions

The manuscript was written by R.E.H., D.L.W., and Y.Y. with contributions from other authors. All authors have given approval to the final version of the manuscript.

Notes

The authors declare no competing financial interest.

■ ACKNOWLEDGMENTS

The authors thank Kanako Hatanaka, Ryo Takahashi, Maho Honda-Yamagishi, Takanori Kawaguchi, Mitsukane Yoshinaga, Takashi Yoshizumi, Shingo Sekine, Shinichi Nishimoto, Takehiko Kato, and Tomoyuki Hata of Taisho Pharmaceuticals for technical assistance; Sean McKenna and Yikang Wang of Vernalis for support in synthesis; and the staff at Diamond Light Source and Soleil synchrotrons for help with crystallographic data collection.

■ ABBREVIATIONS

LpxC, UDP-3-*O*-acyl-*N*-acetylglucosamine deacetylase; MIC, minimum inhibitory concentration; PAβN, phenylalanine-arginine β-naphthylamide; UDP-GlcNAc, uridine diphosphate *N*-acetylglucosamine; IPTG, isopropyl β-D-1-thiogalactopyranoside; HEPES, 4-(2-hydroxyethyl)-1-piperazineethanesulfonic acid; RT, retention time; MMP, matrix metalloprotease; boc, *tert*-butoxycarbonyl; $(BOC)_2O$, di-*tert*-butyl dicarbonate; HATU, *O*-(7-azabenzotriazol-1-yl)-*N*,*N*,*N*′,*N*′-tetramethyluronium hexafluorophosphate; TBAF, tetra-*n*-butylammonium fluoride; THP, tetrahydropyranyl; TMAD, 3-(dimethylcarbamoylimino)-1,1-dimethylurea; TIPS, triisopropylsilyl

■ REFERENCES

(1) Hofer, U. The cost of antimicrobial resistance. *Nat. Rev. Microbiol.* **2019**, *17*, 3.
(2) Brown, E. D.; Wright, G. D. Antibacterial drug discovery in the resistance era. *Nature* **2016**, *529*, 336−343.
(3) Chen, A. Y.; Adamek, R. N.; Dick, B. L.; Credille, C. V.; Morrison, C. N.; Cohen, S. M. Targeting metalloenzymes for therapeutic intervention. *Chem. Rev.* **2019**, *119*, 1323−1455.
(4) Erwin, A. L. Antibacterial drug discovery targeting the lipopolysaccharide biosynthetic enzyme Lpxc. *Cold Spring Harb. Perspect. Med.* **2016**, *6*, No. a025304.
(5) Kalinin, D. V.; Holl, R. Lpxc inhibitors: A patent review (2010-2016). *Expert Opin. Ther. Patents* **2017**, *27*, 1227−1250.
(6) Raetz, C. R.; Reynolds, C. M.; Trent, M. S.; Bishop, R. E. Lipid a modification systems in gram-negative bacteria. *Annu. Rev. Biochem.* **2007**, *76*, 295−329.
(7) Raetz, C. R. H.; Whitfield, C. Lipopolysaccharide endotoxins. *Annu. Rev. Biochem.* **2002**, *71*, 635−700.
(8) Krause, K. M.; Haglund, C. M.; Hebner, C.; Serio, A. W.; Lee, G.; Nieto, V.; Cohen, F.; Kane, T. R.; Machajewski, T. D.; Hildebrandt, D.; Pillar, C.; Thwaites, M.; Hall, D.; Miesel, L.; Hackel, M.; Burek, A.; Andrews, L. D.; Armstrong, E.; Swem, L.; Jubb, A.; Cirz, R. T. Potent Lpxc inhibitors with in vitro activity against multidrug-resistant pseudomonas aeruginosa. *Antimicrob. Agents Chemother.* **2019**, *63*, e00977.
(9) Cohen, F.; Aggen, J. B.; Andrews, L. D.; Assar, Z.; Boggs, J.; Choi, T.; Dozzo, P.; Easterday, A. N.; Haglund, C. M.; Hildebrandt, D. J.; Holt, M. C.; Joly, K.; Jubb, A.; Kamal, Z.; Kane, T. R.; Konradi, A. W.; Krause, K. M.; Linsell, M. S.; Machajewski, T. D.; Miroshnikova, O.; Moser, H. E.; Nieto, V.; Phan, T.; Plato, C.; Serio, A. W.; Seroogy, J.; Shakhmin, A.; Stein, A. J.; Sun, A. D.; Sviridov, S.; Wang, Z.; Wlasichuk, K.; Yang, W.; Zhou, X.; Zhu, H.; Cirz, R. T. Optimization of Lpxc inhibitors for antibacterial activity and cardiovascular safety. *ChemMedChem* **2019**, *14*, 1560−1572.
(10) Shen, S.; Kozikowski, A. P. Why hydroxamates may not be the best histone deacetylase inhibitors—what some may have forgotten or would rather forget? *ChemMedChem* **2016**, *11*, 15−21.
(11) Vandenbroucke, R. E.; Libert, C. Is there new hope for therapeutic matrix metalloproteinase inhibition? *Nat. Rev. Drug Discovery* **2014**, *13*, 904−927.
(12) Montgomery, J. I.; Brown, M. F.; Reilly, U.; Price, L. M.; Abramite, J. A.; Arcari, J.; Barham, R.; Che, Y.; Chen, J. M.; Chung, S. W.; Collantes, E. M.; Desbonnet, C.; Doroski, M.; Doty, J.; Engtrakul, J. J.; Harris, T. M.; Huband, M.; Knafels, J. D.; Leach, K. L.; Liu, S.; Marfat, A.; McAllister, L.; McElroy, E.; Menard, C. A.; Mitton-Fry, M.; Mullins, L.; Noe, M. C.; O'Donnell, J.; Oliver, R.; Penzien, J.; Plummer, M.; Shanmugasundaram, V.; Thoma, C.; Tomaras, A. P.; Uccello, D. P.; Vaz, A.; Wishka, D. G. Pyridone methylsulfone hydroxamate Lpxc inhibitors for the treatment of serious gram-negative infections. *J. Med. Chem.* **2012**, *55*, 1662−1670.
(13) Clayton, G. M.; Klein, D. J.; Rickert, K. W.; Patel, S. B.; Kornienko, M.; Zugay-Murphy, J.; Reid, J. C.; Tummala, S.; Sharma, S.; Singh, S. B.; Miesel, L.; Lumb, K. J.; Soisson, S. M. Structure of the bacterial deacetylase Lpxc bound to the nucleotide reaction product reveals mechanisms of oxyanion stabilization and proton transfer. *J. Biol. Chem.* **2013**, *288*, 34073−34080.
(14) Zhang, J.; Chan, A.; Lippa, B.; Cross, J. B.; Liu, C.; Yin, N.; Romero, J. A.; Lawrence, J.; Heney, R.; Herradura, P.; Goss, J.; Clark, C.; Abel, C.; Zhang, Y.; Poutsiaka, K. M.; Epie, F.; Conrad, M.; Mahamoon, A.; Nguyen, K.; Chavan, A.; Clark, E.; Li, T. C.; Cheng, R. K.; Wood, M.; Andersen, O. A.; Brooks, M.; Kwong, J.; Barker, J.; Parr, I. B.; Gu, Y.; Ryan, M. D.; Coleman, S.; Metcalf, C. A., 3rd Structure-based discovery of Lpxc inhibitors. *Bioorg. Med. Chem. Lett.* **2017**, *27*, 1670−1680.
(15) Baurin, N.; Aboul-Ela, F.; Barril, X.; Davis, B.; Drysdale, M.; Dymock, B.; Finch, H.; Fromont, C.; Richardson, C.; Simmonite, H.; Hubbard, R. E. Design and characterization of libraries of molecular fragments for use in nmr screening against protein targets. *J. Chem. Inf. Comput. Sci.* **2004**, *44*, 2157−2166.
(16) Chen, I. J.; Hubbard, R. E. Lessons for fragment library design: Analysis of output from multiple screening campaigns. *J. Comput. Aided Mol. Des.* **2009**, *23*, 603−620.
(17) Hubbard, R. E.; Davis, B.; Chen, I.; Drysdale, M. J. The seeds approach: Integrating fragments into drug discovery. *Curr. Top Med. Chem.* **2007**, *7*, 1568−1581.
(18) Hubbard, R. E.; Murray, J. B. Experiences in fragment-based lead discovery. *Methods Enzymol.* **2011**, *493*, 509−531.
(19) Credille, C. V.; Dick, B. L.; Morrison, C. N.; Stokes, R. W.; Adamek, R. N.; Wu, N. C.; Wilson, I. A.; Cohen, S. M. Structure−activity relationships in metal-binding pharmacophores for influenza endonuclease. *J. Med. Chem.* **2018**, *61*, 10206−10217.
(20) Lamoree, B.; Hubbard, R. E. Current perspectives in fragment-based lead discovery (fbld). *Essays Biochem.* **2017**, *61*, 453−464.
(21) Erlanson, D. A.; Fesik, S. W.; Hubbard, R. E.; Jahnke, W.; Jhoti, H. Twenty years on: The impact of fragments on drug discovery. *Nat. Rev. Drug Discovery* **2016**, *15*, 605−619.
(22) Hubbard, R. E. Fragment Based Lead Discovery, In *The Handbook of Medicinal Chemistry: Principles and Practice*; The Royal Society of Chemistry, 2015; pp 122−153.
(23) Hubbard, R. E. The Role of Fragment-Based Discovery in Lead Finding, In *Fragment-Based Drug Discovery Lessons and Outlook*, Erlanson, D. A.; Jahnke, W., Eds.; Wiley, 2016; pp 1−36.
(24) Clements, J. M.; Coignard, F.; Johnson, I.; Chandler, S.; Palan, S.; Waller, A.; Wijkmans, J.; Hunter, M. G. Antibacterial activities and characterization of novel inhibitors of Lpxc. *Antimicrob. Agents Chemother.* **2002**, *46*, 1793−1799.
(25) Kabsch, W. Xds. *Acta Crystallogr., Sect. D: Biol. Crystallogr.* **2010**, *66*, 125−132.
(26) Winn, M. D.; Ballard, C. C.; Cowtan, K. D.; Dodson, E. J.; Emsley, P.; Evans, P. R.; Keegan, R. M.; Krissinel, E. B.; Leslie, A. G. W.; McCoy, A.; McNicholas, S. J.; Murshudov, G. N.; Pannu, N.

https://dx.doi.org/10.1021/acs.jmedchem.0c01215
J. Med. Chem. XXXX, XXX, XXX−XXX

S.; Potterton, E. A.; Powell, H. R.; Read, R. J.; Vagin, A.; Wilson, K. S. Overview of the ccp4 suite and current developments. *Acta Crystallogr., Sect. D: Biol. Crystallogr.* **2011**, *67*, 235−242.
(27) Schüttelkopf, A. W.; van Aalten, D. M. F. Prodrg: A tool for high-throughput crystallography of protein-ligand complexes. *Acta Crystallogr., Sect. D: Biol. Crystallogr.* **2004**, *60*, 1355−1363.
(28) Murshudov, G. N.; Vagin, A. A.; Dodson, E. J. Refinement of macromolecular structures by the maximum-likelihood method. *Acta Crystallogr., Sect. D: Biol. Crystallogr.* **1997**, *53*, 240−255.
(29) Emsley, P.; Cowtan, K. Coot: Model-building tools for molecular graphics. *Acta Crystallogr., Sect. D: Biol. Crystallogr.* **2004**, *60*, 2126−2132.
(30) Levy, D. E.; Lapierre, F.; Liang, W.; Ye, W.; Lange, C. W.; Li, X.; Grobelny, D.; Casabonne, M.; Tyrrell, D.; Holme, K.; Nadzan, A.; Galardy, R. E. Matrix metalloproteinase inhibitors: A structure-activity study. *J. Med. Chem.* **1998**, *41*, 199−223.
(31) CLSI. Performance Standards for Antimicrobial Susceptibility Testing. In *CLSI Supplement M100-S26*, 27th ed.; Wayne, P. A., Ed.; Clinical and Laboratory Standards Institute, 2017.

https://dx.doi.org/10.1021/acs.jmedchem.0c01215
J. Med. Chem. XXXX, XXX, XXX−XXX